HELSINKI UNIVERSITY OF TECHNOLOGY
Department of Chemical Technology

Jani Turku

NANOSTRUCTURES IN BLOCK COPOLYMER THIN FILMS

Thesis for the degree of Master of Science in Technology.

Espoo, 1 October 2002

Supervisor:

Professor Jukka Seppälä

Instructor:

Professor Olli Ikkala

PREFACE

This Master's Thesis has been carried out in the laboratory of Optics and Molecular Materials of the Department of Engineering Physics and Mathematics at The Helsinki University of Technology between January and September 2002.

I am grateful for the opportunity to be able to work and use the facilities as a part of The Polymer Physics Group. I would like to express my utmost gratitude for Professor Olli Ikkala of the Department of Engineering Physics and Mathematics at The Helsinki University of Technology for the support and comments during the work process. Especially I would like to thank all the members of Polymer Physics Group for a friendly and inspiring atmosphere both in and out of the office.

M.Sc. Arja Paananen of VTT Biotechnology was an invaluable resource of knowledge in the field of Atomic Force Microscopy. She is to thank for the endless orientation sessions and numerous troubleshooting solutions.

I am also very thankful for Professor George Krausch, Diplom Physicist Armin Knoll and Diplom Chemist Nicolaus Rehse of The Department of Physical Chemistry II at The University of Bayreuth. They supported me with ideas, suggestions, and constructive criticism about my thesis, but first and foremost about solvent annealing method.

Finally I would like to thank my family, friends and everybody for supporting me on the way. Especially, Julia, thank you for being there for me.

Espoo, 1 October

Jani Turku

TEKNILLINEN KORKEAKOULU
Kemian tekniikan osasto

DIPLOMITYÖN TIIVISTELMÄ

Tekijä	Päiväys
Jani Turku	01.10.2002
	Sivumäärä 73
Työn nimi: Nanostructures in Block Copolymer Thin Films	
Professuuri: Polymeeriteknologia	Koodi: Kem-100
Työn valvoja: Professori Jukka Seppälä	
Työn ohjaaja: Professori Olli Ikkala	

Työssä tutkittiin lohkopolymeerin itseorganisoituneita ohutkalvoja atomivoimamikroskoopilla (eng. Atomic Force Microscope, AFM). Työssä tutkittiin kolmea lohkopolymeeriä sekä eri alustojen ja käsittelytapojen vaikutusta syntyvään rakenteeseen.

Alustavaksi koesarjaksi valittiin sylinterimäinen itseorganisoitunut polystyreeni-*lohko*-polymetyylimetakrylaatti, koska sen käyttäytyminen ohuissa kalvoissa tunnetaan. Lisäksi tämän materiaalin AFM-faasikuvissa on riittävä kontrasti, jotta mikrofaasierottuneet lohkot pystytään erottamaan toisistaan. Lämpökäsittelyllä ultraohueen (paksuus vähemmän kuin yksi toistoetäisyys) kalvoon syntyi nk. matomaisten lyhyiden sylinterien ja pallojen pintarakenne. Liuoskäsittelyllä sylinterit asettuivat samansuuntaisesti polaarisen alustan kanssa. Vaihdolla polystyreenisylintereistä polymetyylimetakrylaattimatriisissa polymetyylimetakrylaattisylintereihin polystyreenimatriisissa ei ollut vaikutusta syntyvään morfologiaan. Myöskään alustan valinnalla, pii tai polyimidi, ei ollut merkittävää vaikutusta syntyvään rakenteeseen.

Seuraavaksi tutkittiin polystyreeni-*lohko*-poly-4-vinyylipyridiiniä, jolla on mahdollisuus rakentaa hierarkkisia rakenteita. Sylinterimäistä itseorganisoitunutta lohkopolymeeriä tutkittiin ja todettiin ettei AFM:ssä kontrasti riitä pinnalla olevan polystyreenikerroksen takia. Pyyhkäisyelektronimikroskoopilla tutkittiin liuoskäsiteltyjä kalvoja ja rakenteen todettiin olevan samansuuntainen alustan kanssa.

Hierarkkisia rakenteita valmistettiin liittämällä poly-4-vinyylipyriidinilohkoon pentadekyylifenoli (eng. pentadecylphenol, PDP). PDP kiinnittyi vetysidoksella pyridiinirenkaan typpiatomiin. Tavoitteena oli valmistaa hierarkkisia rakenteita kompleksoimalla lohkopolymeeriä. Valittiin koostumus, jolla bulkissa olisi sylinterin sisässä oleva lamellinen rakenne. Valmistetuissa ohutkalvoissa havaittiin terassirakenteita, joka viittaisi lamellaariseen rakenteeseen. Työssä on esitetty kolme tulkintaa rakenteelle ja sen synnylle. Todennäköisin rakenne on hierarkkinen, jossa lamellien sisässä on lamellaarinen rakenne. Epätodennäköisempenä vaihtoehtoina on lamellirakenne, jossa joko PDP on poistunut rakenteesta tai pintavaikutusten ansiosta rakenteesta on tullut lamellaarinen.

Tässä työssä on havaittu ensimmäiset todisteet hierarkkisista rakenteista ohutkalvoissa ja lisätutkimuksia tarvitaan rakenteen varmentamiseksi.

HELSINKI UNIVERSITY OF TECHNOLOGY
Department of Chemical Technology

ABSTRACT OF MASTER'S THESIS

Author	Date
Jani Turku	1 October 2002
	Pages: 73
Title of thesis: Nanostructures in Block Copolymer Thin Films	
Chair: Polymer Technology	Chair Code: Kem-100
Supervisor: Professor Jukka Seppälä	
Instructor: Professor Olli Ikkala	

Atomic Force Microscope (AFM) was introduced as a tool for the study of block copolymer thin films. Three different block copolymer polymer thin film systems were studied on two different substrate materials with two different annealing methods.

First AFM was established as a method with a material, poly(styrene)-*block*-poly(methyl methacrylate), which is widely researched in the field. The phase contrast in AFM was sufficient to distinguish the phases. With thermal annealing a structure of worm-like cylinders and spheres was observed in ultrathin film with thickness less than a complete repeat thickness. With solvent annealing the structure was parallel to the polar substrate (silicon or poly(imide)). Reverting the morphology from poly(methyl methacrylate) cylinders in poly(styrene) matrix to poly(styrene) cylinders in poly(methyl methacrylate) matrix showed no significant change in the morphology.

After that thin films were manufactured with material that allow structural hierarchy upon introducing. Pure poly(styrene)-*block*-poly(4-vinyl pyridine) was studied with AFM and it was concluded that films with thermal or solvent annealing do not provide sufficient phase contrast to identify the structure due to the poly(styrene) layer on top of the film. Scanning Electron Microscope was utilised in identification and the structure was concluded to be cylinders parallel to the substrate.

Hierarchical structures were prepared by introducing pentadecylphenol (PDP) to poly(styrene)-*block*-poly(4-vinyl pyridine). PDP attaches to the nitrogen atom of the pyridine ring. The expected bulk structure of lamellar-within-cylindrical produced films with islands and holes, which highly indicates to a lamellar structure. Three possible explanations are given, the most probable being the formation of hierarchical of lamellar-within-lamellar due to the side-chain crystallisation. The more unlikely explanations are that a non-hierarchical lamellar structure is formed, either because PDP has left the structure or the surface effects demand a lamellar morphology.

In the scope of this thesis the first evidence of hierarchical structure in thin films is observed. Further studies are needed to verify the morphologies.

All
great deeds
and all
great thoughts
have a
ridiculous beginning.

- A. Camus

CONTENTS

LIST OF SYMBOLS AND ABBREVIATIONS USED IN TEXT

AFM	Atomic Force Microscope
BCC	Body-centred cubic
E_0	Electric field
F	Composition of block copolymer
F	Free energy of dielectric body
F_0	Orientation independent electrical contribution to the free energy of dielectric body
F_{el}	Orientation dependent electrical contribution to the free energy of dielectric body
FE-SEM	Field Emission Scanning Electron Microscope
H	Magnetic field
h	Local film thickness
HUT	Helsinki University of Technology
IUPAC	International Union of Pure and Applied Chemistry
k	Boltzmann constant
MDP	Multidomain Polymer
N	Degree of polymerisation
N_i	Number of segments of component i
ODT	Order-disorder transition
P	Polarisation inside the dielectric body
p	partial pressure
P4VP	Poly(4-vinyl pyridine)
PD	Polydispersity
PDP	Pentadecylphenol
PEE	Poly(ethyleneoxide)
PMMA	Poly(methyl metacrylate)
PS	Poly(styrene)
PVCH	Poly(vinyl-cyclohexane)
q	The domain strength of the multidomain polymer
rpm	Revolutions per minute

SEM	Scanning Electron Microscope
SPM	Scanning Probe Microscope
T	Temperature
TEM	Transmission Electron Microscope
T_G	Glass-transition temperature
TMBA	Too many bloody abbreviations
V	Volume
w-%	Weight percent
Z	Axis of magnetic symmetry
z	Lattice coordination number

λ	Wavelength
θ	Angle
ε_{ext}	Dielectric constant of the surrounding media
ε	Permittivity in vacuum
ε_{ij}	Contact energy between blocks *i* and *j*
χ	Flory-Huggins interaction parameter
ΔG_{mix}	Free energy of mixing
ΔH_{mix}	Enthalpy of mixing
ΔS_{mix}	Entropy of mixing
φ	Volume fraction
κ	Polarisability
$\chi_{\parallel}$	Molar magnetic susceptibility paraller to the axis
$\chi_{\perp}$	Molar magnetic susceptibility perpendicular to the axis
ω	Characteristic frequency

I THEORETICAL PART

1 INTRODUCTION

"God does not throw dice", said Albert Einstein. What he meant was that Mother Nature has its own subtle way of organising things.

Self-organisation is seen in nature in many mesoscale objects such as liquid crystals, liposomes, surfactants, lipids, and micelles. Many of the necessities of life are made possible only by self-organising materials. [1, 2]

Without altering the chemical composition, introduction of the desired microstructure can enhance or even create outstanding properties from a traditional material. Self-organisation provides versatile means to create desired nanostructures in bulk materials or at interfaces with potential applications in biomaterials, optics and microelectronics. [1, 3-6]

Block copolymers represent an important class of microstructurally engineered materials because their morphology and dynamics can be systematically controlled by choosing the blocks' compositions and relative lengths. [7, 8] Self-organising block copolymer materials have important commercial applications as thermoplastic elastomers, compatibilisers in polymer blends, and gas and solution separation applications. Today block copolymers are found in everyday applications such as upholstery foam, pressure-sensitive adhesives, oil and asphalt additives, high-impact plastics, and in a variety of automobile parts. [7, 8] In the near-future more advanced applications based on the block copolymers can be expected, for example in the areas of nanoscale lithography, selectively permeable membranes, and electronics. [8-10]

Thin films are the basis of today's information technology society and applications vary from window coatings to microchips. The electronics industry has a keen interest in developing new methods for nanofabrication in order that the long-term trend of

building ever smaller, faster and less expensive devices may continue. It would be natural evolution of microelectronics to gradually become nanoelectronics. The exploration of alternative technologies for making future nanochips is under intensive research and block copolymer thin films may hold the key to the next breakthrough. [1, 2]

The ultimate goal for block copolymer thin films is to develop a method of manufacturing controlled structures starting from molecules and polymers and advancing to nanoscale, mesoscale and all the way to the macroscale. [1, 2, 6]

In the scope of this work, Atomic Force Microscope (AFM) was introduced as a tool for analysing block copolymer thin films. Three different block copolymer polymer thin film systems were studied on two different substrate materials with two different annealing methods.

First the AFM was established as a method with poly(styrene)-*b*-poly(methyl methacrylate) (PS-*b*-PMMA) of cylindrical morphology. Secondly thin films were manufactured with material that allows structural hierarchy upon introducing. Poly(styrene)-*b*-poly(4-vinyl pyridine) (PS-*b*-P4VP) formed lamellar structures with the introduction of pentadecylphenol (PDP) that were interpreted to be hierarchical lamellar-within-lamellar structures.

2 POLYMER STRUCTURES AND ORDERING

2.1 Structures of Homopolymers

Polymer is a Greek word originating from words 'poly' meaning many and 'mer' meaning part. Polymers are large, usually chainlike, molecules that are built from smaller molecules called monomers. Monomers are linked by strong bonds to form polymers. Usually the bond is covalent, but recently other types of bonds have been incorporated also. [11, 12] A molecule with only a few constitutional repeat units is called an oligomer. In oligomers, the physical properties may vary upon addition or removal of one or more repeat units. According to IUPAC definition, polymer provides a set of properties that do not vary markedly with the addition of one or a few of constitutional repeat units. [13] The amount of repeat units can be very high and thus the size of the polymer can be very large. Therefore, polymers are also called macromolecules. [14, 15]

When a polymer consists of only one constitutional repeat unit, it is called a homopolymer. Typical homopolymer structure can be linear, branched or cross-linked. Graft copolymers consist of branches attached to a main chain. Various architectures can be seen in Figure 1. [15]

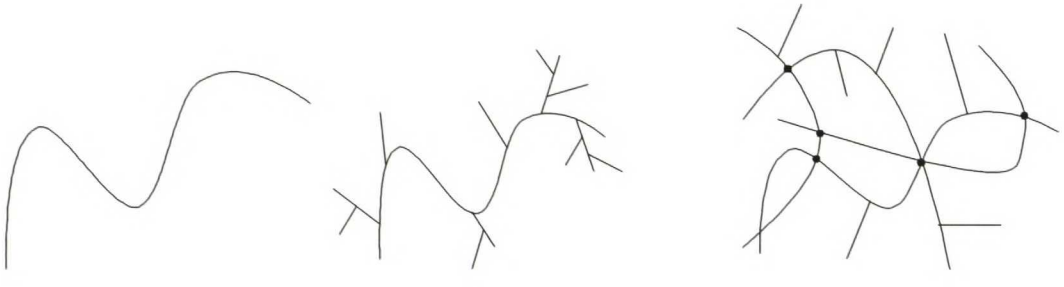

Figure 1. Some homopolymer architecture from left to right: linear, branched and crosslinked. Crosslinks are marked with black dots. [15].

2.2 Structures of Block Copolymers

A copolymer is formed, when the polymer chain consists of two or more different repeat units. They may be distributed irregularly as in random copolymers or form alternating copolymers. Block copolymers are produced by joining at least two chemically distinct polymer blocks together. [8, 16, 17]

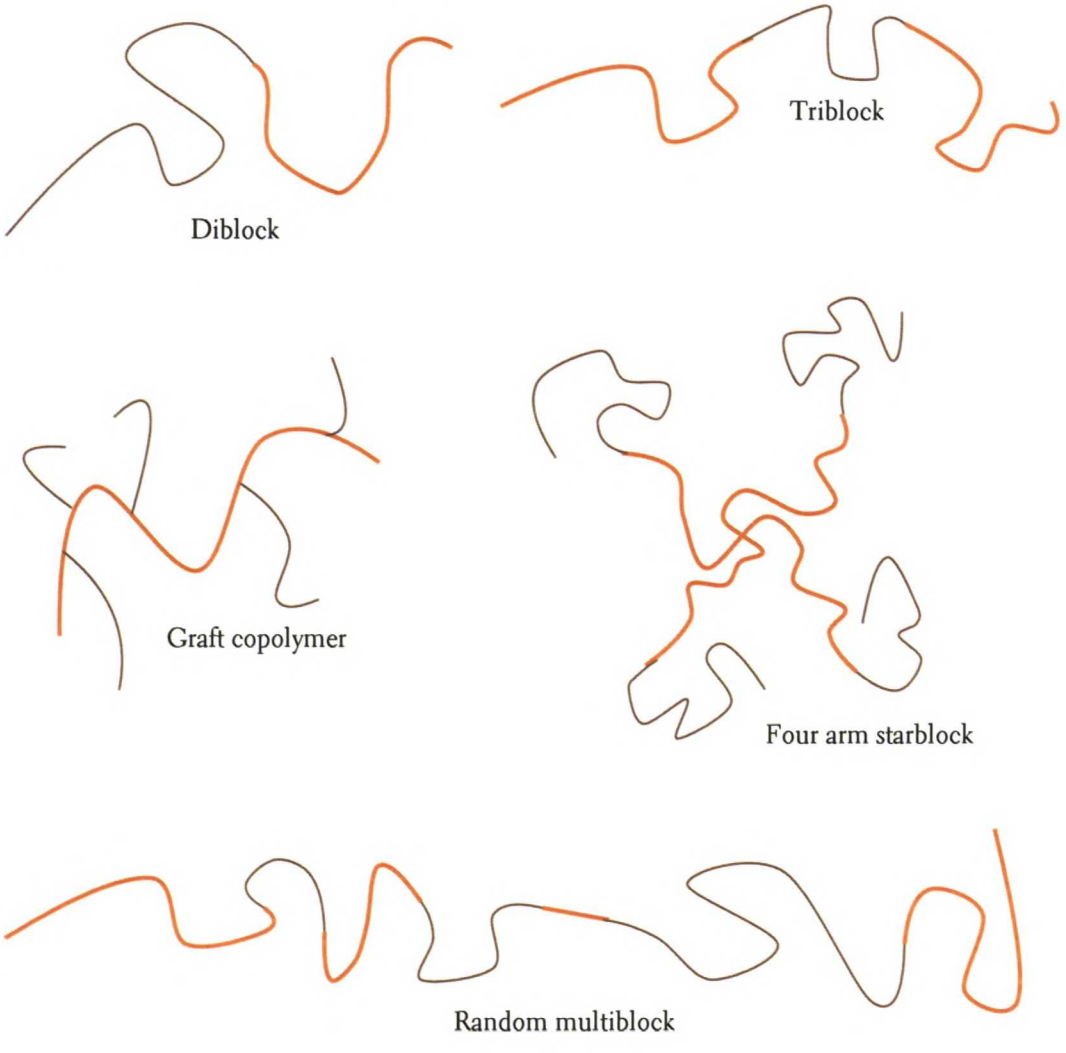

Figure 2. Some typical block copolymer architectures. [17]

The molecular architectures of block copolymers can be controlled by the synthesis procedure. A basic classification of molecular architectures can be based on two parameters: I) the number of chemically distinct blocks, and II) linear versus branched sequencing of the blocks. The simplest possible structure is diblock, but it is possible to prepare triblock, multiblock, starblock, and graft copolymers as illustrated in Figure 2. In recent studies, for diblocks, there are structures-within-structures [18], and for multiblocks there are more exotic architectures available upon complexation with suitable additives such as helical strands surrounding cylinders, coaxial cylinders or cocentric spherical domains in body-centred-cubic structure. [8, 17, 19-21]

3 SELF-ORGANISATION AND NANOSCALE STRUCTURES OF BLOCK COPOLYMERS IN BULK

3.1 Self-Organisation

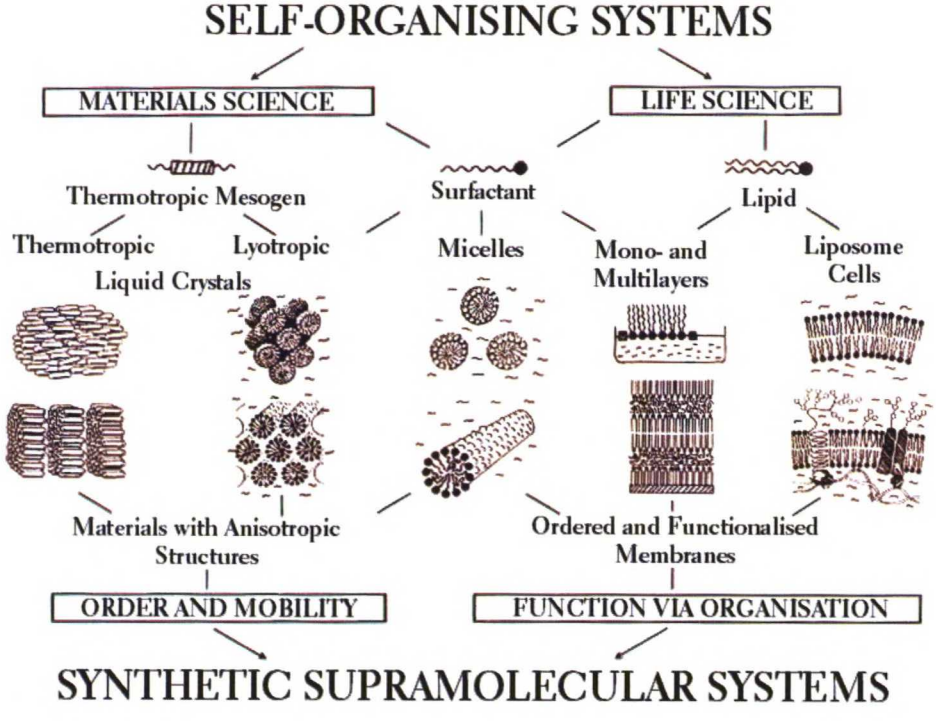

Figure 3. Self-organisation and supramolecular structures in material sciences and life sciences. [22] The structure formation in surfactant or lipid systems is based on hydrophilic/hydrophobic effects, whereas in liquid crystals formation is due to the shape persistence of the covalently bonded mesogenic moieties.

In self-organising materials the structural order is created by combining competing molecular interactions (Figure 3). Typical repulsive interactions are hydrophobic/ hydrophilic or nonpolar/polar effects, and attractive interactions are hydrogen bonding, coulombic interactions, and van der Waals forces. Combinations of the aforementioned attractive and repulsive interactions create minima in the local free energy. As an example of combination, to act as enzymes proteins require specific chemical sequences, but they must fold into a required shape to create a substrate-specific docking

site. The protein itself must avoid aggregation to remain in solution or incorporate itself into a membrane layer. [3]

In polymer molecules, because the building blocks are covalently tethered together, the change from one conformation to another can take place only in certain ways as specified by the allowed bond rotations. The values of these free energy barriers are entailed by the details of competing interactions. [3]

As suggested by the structures and functions of biological matter [23, 24], in recent years similar hierarchical self-organization has been pursued also in synthetic materials. According to Muthukumar *et al.* [3] there are three guiding principles to impose structural order over many length scales in self-organising structures. Materials designed with only one process in mind create supramolecular structures of certain length scale only. Combining several interactions can create order over many length scales.

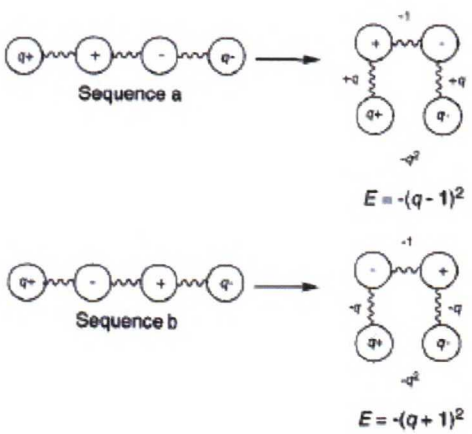

Figure 4. Different internal sequences have different energies. Sequence (a) leads to a less stable structure than a chain with sequence (b). [3]

The first principle is of competing interactions and sequences. Let's consider a hypothetical and oversimplified multidomain polymer (MDP) consisting of domains as in Figure 4. Each domain has the desired chemical function. The potential nature of each domain is represented by strength q and a sign. One domain q_1+ and another q_2- are complementary to each other and, if adjacent, will stabilise the structure by energy $q_1 q_2$. Domains of the same sign will destabilise the structure. Domains have several different possibilities to sequence internally. Unfavourable structures can be

stabilised by carefully promoting interactions among domains of a MDP with underlying desired sequences. [3]

The second principle is of entropic frustration and topological dereliction. There are three ways to choose and pursue to the desired structure through free energy. First is to considerably reduce the number of topological states for a given number of pairings between domains by making the sequence tighter through reduction of the spacer length. Second is to tune the value of pairing energy to smaller values for example by using weaker interactions. Third is to provide an external field to the evolving system at opportune times to guide the system to reach the desired final structures. [3]

The third guiding principle is the spontaneous selection of primary length scales. Many polymeric liquids self-organise spontaneously into ordered structures with well-defined symmetry and dominant characteristic lengths. The mechanism of selection of a primary length scale is generic. [3]

3.2 Self-Organisation in Diblock Copolymers

Block copolymers have remarkable properties to self-organise in the melt or in the bulk into a variety of ordered structures as seen in Figure 5. This collective self-organisation produces spatially periodic composition patterns that can exhibit considerable complexity. These patterns are commonly referred to as microphases, mesophases or nanophases, depending on the length-scale. As the constituent blocks of polymers are typically immiscible, the self-organisation is induced on a scale that is directly related to the size of the copolymer chains. The length-scale of these domains is typically 10-100 nm, depending on the material. [8, 17, 25, 26]

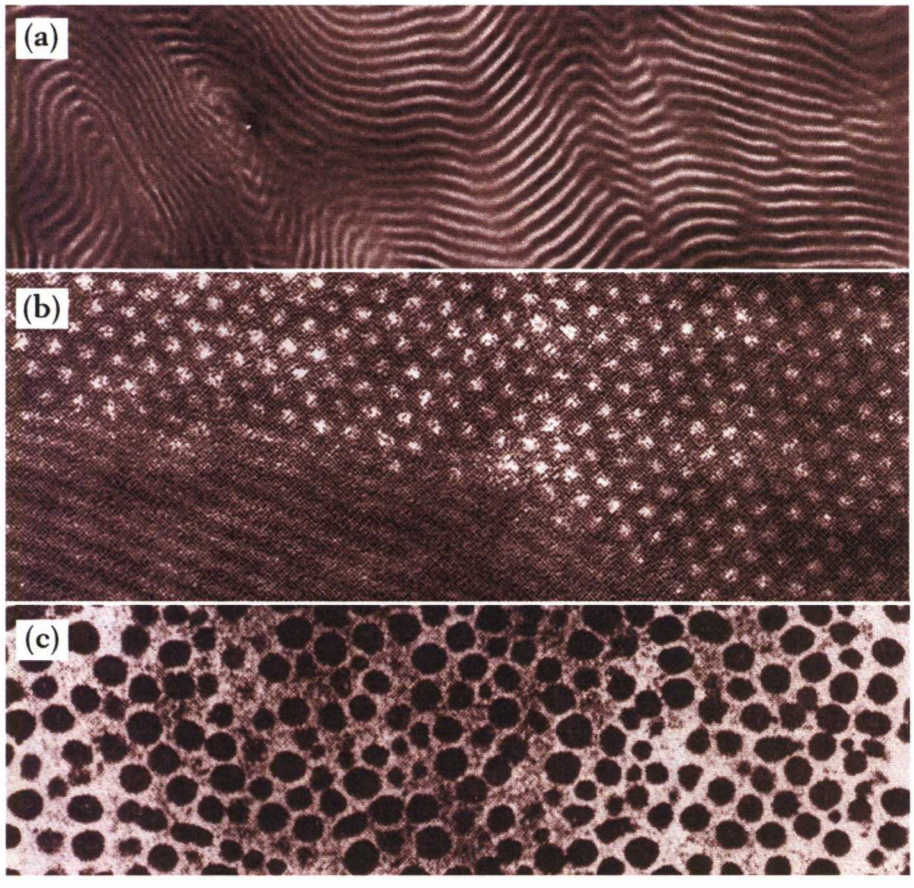

Figure 5. Different microstructures shown by Transmission Electron Microscopy (TEM): (a) lamellar poly(styrene)-*b*-poly(isoprene), (b) cylindrical self-organization of hexagonal poly(styrene)-*b*-poly(2-vinyl pyridine) cylinders, (c) body-centred-cubic poly(styrene)-*b*-poly(butadiene)-*b*-poly(styrene) spheres. [17] The typical periodicities are in the range of 10-100 nm, depending on the molecular weight of the polymeric blocks.

The phase behaviour of bulk diblock copolymers is determined by experimentally controllable factors: the overall degree of polymerisation N, the architectural constraints, the volume fraction of one component, and the A-B segment-segment interaction parameter χ. [7] In normal polymerisation process, the chemical kinetics results in a relatively large distribution of molecular weights, and in block copolymers this results in compositional heterogeneity. Compositional homogeneity is assured by the careful consideration of polymerisation process. Therefore usually polymers are usually manufactured by anionic living polymerisation and the polydispersity is well below 1.3. [8]

If N is sufficiently large, it is impossible to obtain equilibrium structure in finite time, but the chains may by local compositional ordering find a local free energy minimum. [7]

3.3 Macrophase and Microphase Separation

3.3.1 Melt Behaviour in Mixtures

First a mixture of polymers needs to be discussed. In the system of mixing two or more separate polymers, the Gibbs free energy of mixing ΔG_{mix} can be derived [14] from the second law of thermodynamics:

$$\Delta G_{mix} = \Delta H_{mix} - T\Delta S_{mix} \qquad (1)$$

where ΔG_{mix} = Free energy of mixing

ΔH_{mix} = Enthalpy of mixing

ΔS_{mix} = Entropy of mixing

For polymer systems, the free energy of mixing per unit can be expressed as [27]:

$$\frac{\Delta G_{mix}}{nkT} = \frac{\varphi}{N_1}\ln\varphi + \frac{1-\varphi}{N_2}\ln(1-\varphi) + \chi\varphi(1-\varphi) \qquad (2)$$

where φ = Volume fraction of polymer 1

N_i = Number of segments of equal size of the polymer i

k = Boltzmann constant

The first two terms are the negative and comprise of entropy part that tends to maximise the disorder and the last term, which is positive, wants to minimise the interaction energy. The requirement of $\Delta G_{mix} < 0$ is a necessary but not sufficient condition for miscibility for polymer systems. [14, 27]

Consider a pure system containing molecules of type A only and put it in the system containing only molecules of type B. The corresponding change in interaction energy is given by $\chi_{AB}kT$. Flory-Huggins interaction parameter χ is defined as

$$\chi = \left(\frac{z}{kT}\right)\left[\varepsilon_{AB} - \frac{\varepsilon_{AA} + \varepsilon_{BB}}{2}\right] \tag{3}$$

where z = Lattice coordination number

ε_{ij} = Contact energy between blocks i and j

(The notation ε_{ij} is not to be confused with permittivity ε).

There is a strong tendency for mixing to be endothermic, i.e. strong tendency for a positive χ-parameter. The interaction parameter has a temperature dependence of $\chi \propto 1/T$. The magnitude of the parameter depends on the selection of the blocks. Increasing χ by lowering the temperature favours a reduction in contacts between blocks. If χ is decreased enough for example by increasing the temperature, the entropic factors dominate leading to a homogenously mixed phase.

Unlike binary mixtures of low molecular weight fluids, the entropy of mixing per unit volume of dissimilar polymers is small, varying inversely with molecular weight. Therefore even minor structural or chemical differences between the blocks are sufficient to produce excess free-energy contributions that are usually unfavourable to mixing. As an example, even polymer isotopes, such as poly(styrene) and deuterated poly(styrene), have been demonstrated to be immiscible at sufficiently high molecular weight. [8]

3.3.2 *Microphase Separation in Block Copolymers*

In block copolymers chains constitute of at least of two constituent polymers. If the blocks are immiscible, phase separation cannot be macroscopic, but is induced on a scale that is directly related to the size of the copolymer chains. The length-scale is typically 10-100 nm, depending on the material. [17, 25, 26]

The transition from a homogenous disordered melt into a self-organised melt containing ordered microphase-separated domains takes place as χN is increased: a delicate balance between the energetic and entropic forces produces the order-disorder transition (*ODT*). Transition occurs at a critical value of χN, depending on the length and the composition of the copolymer. [14, 26]

In block copolymers, the phase-separated evolution of microstructure is a result of two competing effects. Dissimilar blocks prefer to segregate due to their inherent chemical incompatibility. The incompatibility of the molecular constituents will favour segregation into two coexisting phases. This macrophase separation is a state of coexistence of bulk phases. In a block copolymer melt, entropic forces from the covalent linkages counterbalance the thermodynamic forces driving separation. [8, 28] These forces, sometimes called chain elasticity, reflect the requirement to keep the dissimilar blocks A and B apart. An entropic restoring force is generated that serves to limit the phase separation between blocks to mesoscopic dimensions, because there are fewer configurations available to extended polymer chains than to those in native randomly coiled state. Microphase separation is driven by the enthalpy of demixing of the components. However, phase separation is limited due to the chemical connectivity of the polymer blocks. Thus, macroscopic segregation cannot occur. [17, 25, 26]

Ordered structures can be controlled either by varying the composition of the copolymer or by the segregation between blocks. Segregation can be controlled via temperature or the degree of the polymerisation. [14]

For symmetric diblock polymer consisting of two blocks, each of length *N*/2, mean field theory predicts the $(\chi N)_{ODT} = 10.5$, compared to $\chi(N/2) = 4.0$ for symmetric polymer blend consisting of two chemically not connected chains of the corresponding length *N*/2. Composition also determines the curvature of the interface between blocks and their packing density. [14, 26]

System strives to satisfy the delicate balance of minimizing the area of contact between incompatible chain segments and maximizing the conformational entropy of the macromolecules. The melt phase behaviour can be characterised by the reduced parameter χN and the composition of the copolymer *f*. If $\chi N < 10.5$, the copolymer

phase is mixed, and the copolymer morphology is homogenous with no microphase separation. [29]

Three regimes have been identified depending on the extent of segregation of the blocks: the weak ($\chi N \leq 10$ - 12), intermediate ($\chi N \approx$ 10-100) and strong segregation ($\chi N \geq 100$) regimes. The precise definition of these limits depends on the criteria used. In the weak segregation limit, the composition profile is approximately sinusoidal. As χN increases, the profile becomes sharper. The evolvement of composition profiles can be seen in Figure 6. For the large values of χN, the block copolymers are strongly segregated. The boundaries delineating the different microphases are expected to be vertical and domains contain essentially pure components. [17, 25, 26, 30]

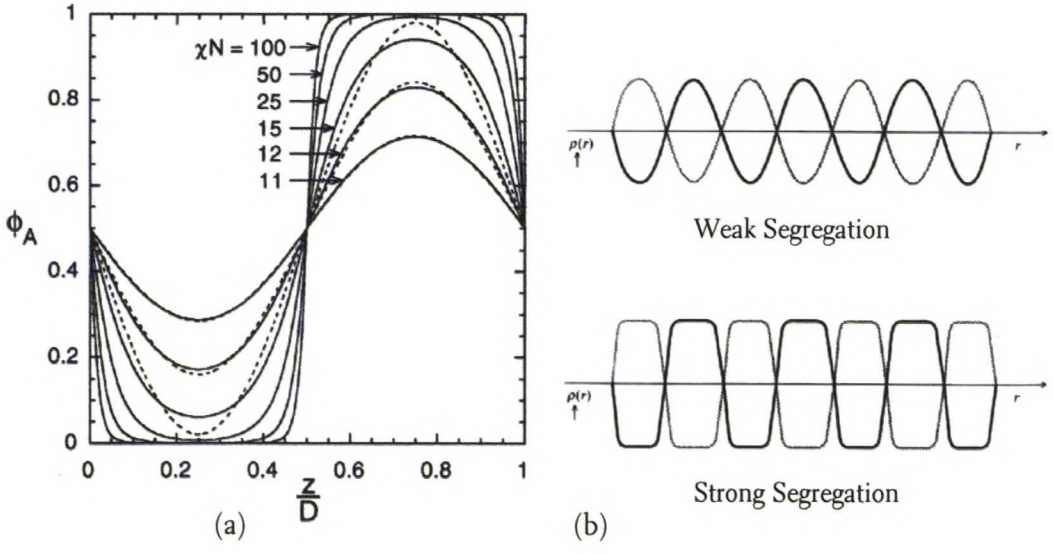

Figure 6. (a) Segment profiles over one period of the lamellar phase of a symmetric diblock melt for various N values. Dashed lines denote first-harmonic approximations for the profiles at N = 11, 12, and 15. [30] (b) Composition profiles in the weak and strong segregation limits compared to the mean. [17]

In weakly segregated polymers, the degree of polymerisation N is an independent variable relevant to the phase behaviour. In strong segregations the limit depends strongly also on the composition. [17, 25, 26, 30]

3.4 Diblock Copolymer Phase Diagram

A diblock copolymer can be ordered or disordered depending on the prevailing circumstances. Phase diagram depicts the nature of transitions from the disordered state to an ordered microphase. Diagram characterises the dependence of the morphological behaviour of the temperature of the specimen and the chemical composition of the diblock copolymer. In order to make phase diagrams universal, the reduced parameter χN is preferred instead of the temperature. This way the diagrams are considered independent of the block copolymer chemistry. [17, 26]

Considering the simplest case, a symmetric diblock polymer, there is no tendency for the interface to curve. Upon microphase separation a lamellar phase is formed as seen in Figure 7c. If the asymmetry of the diblock increases, interfacial curvature increases leading to the formation of phases of hexagonal-packed cylinders (Figure 7b and Figure 7d) or body-centred-cubic spheres of the minority block in majority matrix (Figure 7a and Figure 7e). [17, 25]

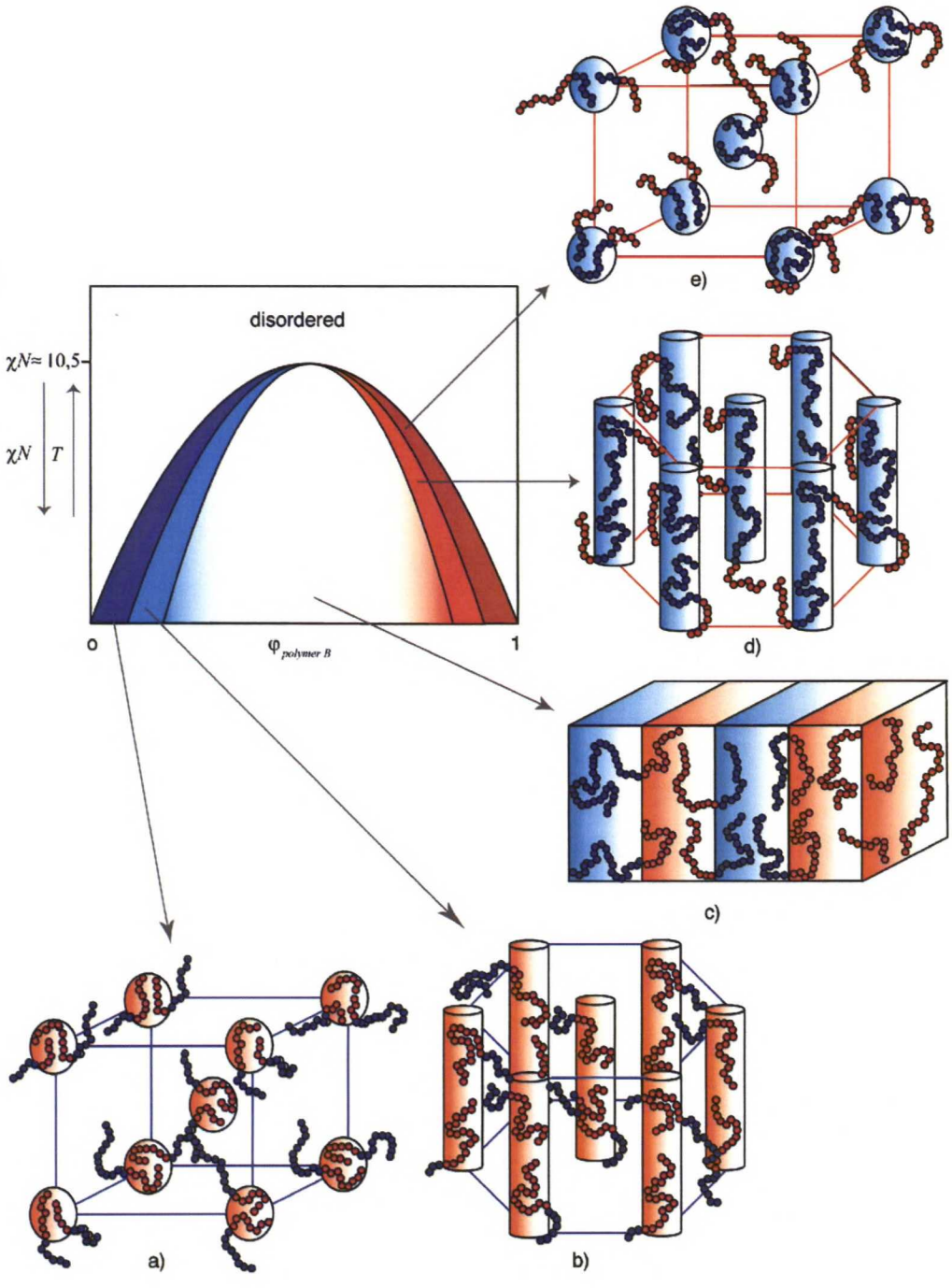

Figure 7. Theoretical phase diagram for diblock copolymer consisting of block A (red) and block B (blue). Diagram can be divided into several areas: (a) A blocks as spheres in the matrix of polymer B blocks in the body-centred-cubic (BCC) lattice. (b) Hexagonally ordered cylinders of A in B matrix. (c) Lamellar structure, where the thickness of layer dependent on the composition. (d) Hexagonally ordered cylinders of B in A matrix. (e) BCC spheres of B in the matrix of A. [7, 31]

In between the hexagonal-packed cylinder and lamellar phase, there is an intricate bicontinuous cubic structure called gyroid, which forms near the *ODT*. Gyroid (Figure 8a) has been established as an equilibrium structure. Another complex phase called perforated layer structure (Figure 8b) is a metastable structure observed during transformations to and from the gyroid structure. [17, 25, 30]

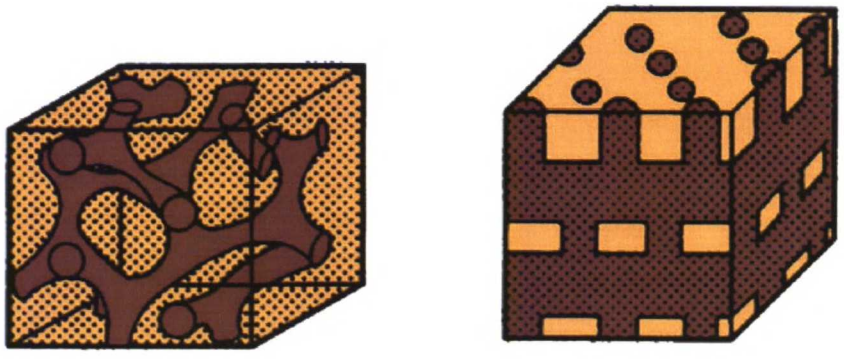

(a) (b)

Figure 8. Complex diblock copolymer phases: (a) bicontinuous gyroid and (b) perforated layers. [17]

Given the morphological complexity of triblock and multiblock copolymers, the complexity of architecture and several thermodynamical possibilities leads to a variety of exotic structures and much more complex phase diagrams. Recent experiments from a number of research groups review these structures in more detail. [17, 20, 21, 32]

3.5 Global Alignment of Self-Organised Structures

Self-organisation allows the control of the nanoscale structures in great detail. In practice the self-organisation of block copolymers lead to local order as seen in Figure 9a. In several applications structures with global alignment are needed. The multidomain structure with domain boundaries is not acceptable. A nearly monodomain structure can be attained by aligning microdomains as in Figure 9b. Most prominently, macroscopic alignment with external fields has been successfully applied to orient block copolymer melts and block copolymer solutions to achieve directional properties, such as transport, optical, and electrical properties. [10, 33-45]

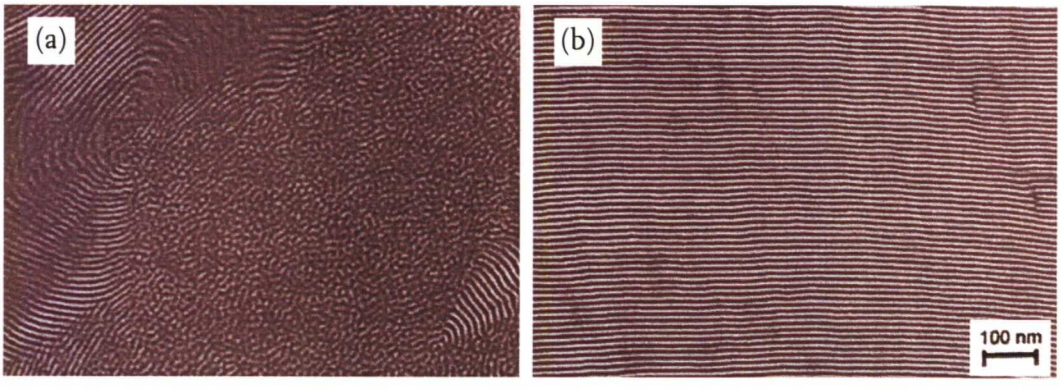

Figure 9. TEM image of polymer microstructure sheared from multidomain structure to a nearly monodomain structure. (a) Before and (b) after large amplitude oscillatory shearing. [10]

For thin films, there are additional constraints due to the surface fields and boundary conditions. Chapter 3 reviews the common alignment methods of bulk copolymers. They are all applicable to thin films also. Chapter 4 concentrates on the special problems of thin films, which are due to the thickness of the film and the effects of different surface fields.

3.5.1 Electric Fields

When a dielectric body with a dielectric constant ε is placed in an electric field $\vec{E}_0$, the polarization difference between the body and the surroundings will induce charges on the surface of the body. These surface charges give rise to a depolarisation field $\vec{E}_p$ superposed on the external field. For an anisotropic body, the surface charges and the depolarisation field depend on the orientation of the body. The resulting electric field is orientation dependent. The state with no electric body present can be used as a reference state. [35] The free energy can be written as:

$$F = F_0 + F_{el} = F_0 - \tfrac{1}{2}\int_V \vec{E}_0 \cdot \vec{P} dV \qquad (4)$$

where F_{el} = Orientation dependent electrical contribution to the free energy

F_0 = Orientation independent electrical contribution to the free energy

$\vec{P}$ = Polarization inside the dielectric body of volume V

The polarisation is proportional to the total electric field:

$$\vec{P} = \kappa \vec{E} = \kappa\left(\vec{E}_0 + \vec{E}_P\right) \qquad (5)$$

where κ = Polarisability (constant for isotropic material)

Polarisability is constant for isotropic material. To evaluate Equation (5), the electric field $\vec{E}$ has to be known, which generally requires solving Maxwell equations for the geometry under consideration. For the simple case of infinitely long cylinder, the solution can be constructed from boundary conditions for the electric field at the interface. The state with the lowest free energy will be one of two orientations, cylinder's axis either parallel or perpendicular to the external field E_0, since only in these cases the torque $\vec{K} = \vec{P} \times \vec{E}_0 = 0$. The resulting difference in the free energy between the two states with the different orientation is:

$$\Delta F = F_{\parallel} - F_{\perp} = \tfrac{1}{2}\vec{E}_0{}^2 \varepsilon_0 \varepsilon_{ext} \left(\frac{\varepsilon}{\varepsilon_{ext}} - 1 \right) \frac{1 - \dfrac{\varepsilon}{\varepsilon_{ext}}}{1 + \dfrac{\varepsilon}{\varepsilon_{ext}}} V \qquad (6)$$

where ε_0 = Permittivity in vacuum

ε_{ext} = Dielectric constant of the surrounding media

Since ΔF is always negative, the orientation of the cylinder parallel to the applied field is the lower free energy state, whether $\varepsilon > \varepsilon_{ext}$ or $\varepsilon <. \varepsilon_{ext}$ [35]

Typical field strength can be in the absence of competing interactions 3 V/ μm [36] and with interfacial tensions between copolymer and electrode surface, the field strength can be typically from 25 to 42 V/μm. [35, 37] The electric field also has an effect on the conformation of the polymers. The effect becomes relevant when the applied field is about a decade higher than those mentioned above. [38]

3.5.2 *Magnetic Fields*

With the development of high magnetic fields, it has become an interesting subject to study the effects of a magnetic field on polymeric materials. Organic molecules, usually having diamagnetic anisotropy, experience torque when an external magnetic field is applied. In the case of an isotropic phase, the torque on single molecule is so small compared to the thermal agitation that it cannot rotate the molecule. [41]

The magnetic orientation is believed to take place by the susceptibility anisotropies. When aggregates are formed by arrangement of anisotropic molecules, the magnetic energies are explained to become large enough for them to be oriented against thermal disordering. [40]

When a crystal, composed of a mole number n of molecules with an axis Z of magnetic symmetry, is placed in magnetic field H, the magnetic anisotropy energy is expressed:

$$E(\theta,H) = -(n/2)\left[\chi_{\perp} + (\chi_{\parallel} - \chi_{\perp})\cos^2\theta\right]H^2 \qquad (7)$$

where θ = Angle between axis Z and field H

$\chi_{\parallel}$ = Molar magnetic susceptibility parallel to the axis

$\chi_{\perp}$ = Molar magnetic susceptibility perpendicular to the axis

(The notation $\chi_{\parallel}$ or $\chi_{\perp}$ is not to be confused with Flory-Huggins interaction parameter χ.)

For a crystal bearing a relation of $\chi_{\parallel} < \chi_{\perp}$, the anisotropy energy $E(\theta,H)$ has a minimum value and the crystal is stabilised when the axis Z is perpendicular to the field $H(\theta = \pi/2)$. As the crystal grows larger with a larger value of the mole number n, the difference of magnetic energies between any direction (θ) and the direction perpendicular to the field $(\theta = \pi/2)$ becomes larger. When the difference of the magnetic energies exceeds the thermal energy, the crystal will be oriented so that the axis Z is oriented perpendicular to the field H. [40]

The simple case is when both the axis and field are restricted in a plane. The axis moves in two-dimensional plane and the degrees of freedom is 1 for the crystal direction, which is represented by the angle θ. The energy $E(\theta,H)$ is a continuous function of angle. [40]

It is well known that liquid crystalline polymers align under magnetic fields due to the large diamagnetic anisotropies provided by aromatic rings. Non-liquid crystalline polymers are usually regarded as being indifferent to the magnetic fields because the polymers lack the ability to form liquid crystalline phases. This fact and the lack of aromatic rings might be unfavourable to magnetic orientation. [42, 43]

Quenching from the nematic state, the induced orientation may be frozen in, and the resulting crystallization does not overtly affect the oriented structure. If the magnetic field is removed while the sample is held in the nematic state, the polymer 'relaxes' and the induced orientation is found to decay away rapidly. [45]

3.5.3 *Oscillatory Shear Flow*

Flow fields have been proposed as one of the means to achieve "single crystal -like" structures in locally ordered materials. Symmetry-breaking field, such as large amplitude oscillatory shear flow (Figure 10), provides an efficient and versatile means of achieving global alignment. [10, 44]

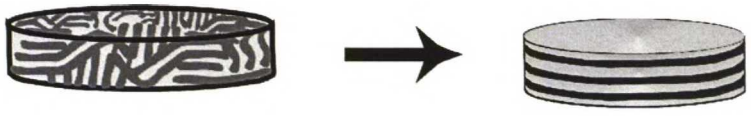

Figure 10. Alignment of self-organised material can be accomplished by a large amplitude oscillatory shear. Before (left) and after shearing (right). [34]

For example in lamellar diblock copolymers it has been shown that two alignments of macroscopic order can be achieved by large-amplitude oscillatory shear flow. Shearing at different frequencies, in conditions above glass-transition and below ODT, at the same temperature and strain amplitudes can produce alignment either parallel or perpendicular to the shear gradient direction. The lamellar phase has the same qualitative stress relaxation behaviour at very low frequencies as a smectic liquid crystal, whereas the cylindrical mesophases of block copolymers share a common low-frequency response with columnar hexagonal phases self-organised from liquid crystals or surfactants. Figure 11 shows the possible orientations. The lower symmetry phases, e.g. BCC spheres and gyroid phases, are classified as solids with regard to their zero-frequency response to stress. [9, 44]

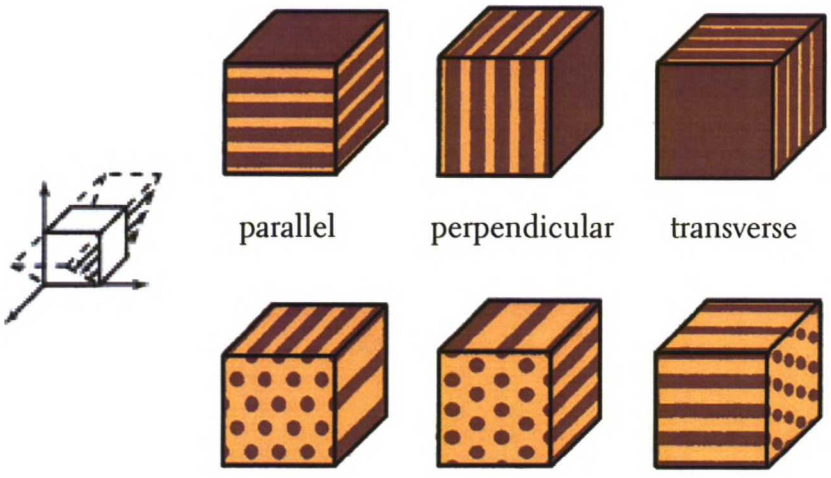

Figure 11. Possible orientations of lamellar (above) and cylindrical (below) phases in respect to shear field: parallel, perpendicular and transverse. [9]

To explain the observed frequency-dependent alignment behaviour, two characteristic frequencies (ω) have been proposed: the frequency above which the distortion of chain conformation dominates the materials' viscoelasticity (ω_c); and the frequency below which the relaxation of domains become significant (ω_d). Between these frequencies the distortion of the nanostructures dominates the viscoelastic response of the material. [10]

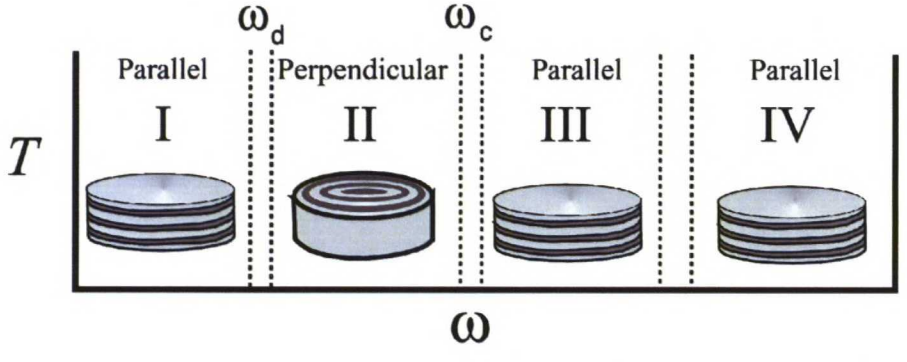

Figure 12. Four different regimes found for PEP-*b*-PEE and PS-*b*-PI systems. [34]

Four frequency regimes (Figure 12) have been found, where different type of alignment dominates in each regime. Perpendicular alignment may be induced by shearing at frequencies that couple with the dynamics of nanostructures, i.e. frequencies too fast for domain-scale relaxation, but slow enough that the chain conformation is relaxed $\omega_d < \omega < \omega_c$ (regime II). Two regimes exist in higher frequencies $\omega > \omega_c$. Both are of parallel alignment, but through two qualitatively different pathways. In regime III, frequencies slightly above ω_c, parallel alignment occurs through a transient orientation distribution that consists of parallel and perpendicular orientations. Frequencies far above ω_c induce parallel alignment through bimodal distributions rich in parallel and transverse orientations. At low frequencies, $\omega < \omega_d$, the alignment tends to be parallel in some systems and perpendicular in others. Within each regime, strain amplitude affects the degree of alignment. [10, 34]

4 BLOCK COPOLYMER THIN FILMS

The effect on structure of confining block copolymers in thin films has been examined, largely using neutron reflectivity and atomic force microscopy. A number of features that result from constraint of reduced dimensionality have been reported, such as the observation of islands and holes at the surface of lamellar block copolymer film, when the thickness of the film is not an integral multiple of the bulk layer spacing. Kinetic and surface effects in thin films can constrain the bulk morphology away from the surface itself. The morphology is combination of several factors, namely the effect of surface fields, film thickness (

Figure 13), solvent evaporation rate, and annealing conditions. [17, 46]

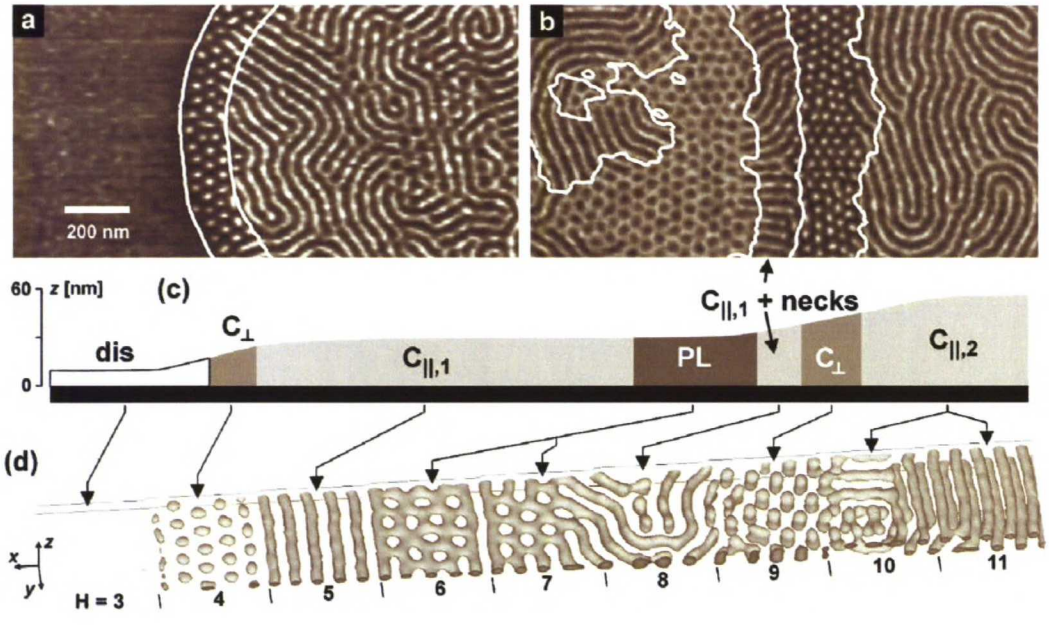

Figure 13. All phases appearing in a single system indicate that the film thickness is a very important factor in controlling the final morphology. (a,b) AFM image of thin poly(styrene)-*b*-poly(butadiene)-*b*-poly(styrene) films on Si substrates after solvent annealing in chloroform vapour. (c) Schematic height profile of the phase images. (d) Computer simulation of similar film with the height profile as in previous. [47]

4.1 Thin Film Boundary Conditions

The behaviour of diblock copolymers in thin films differs from that in the bulk since interfacial interactions control the evolution of their structure. For diblock copolymer films composed of cylindrical or lamellar microdomains, the interfacial interactions dictate the wetting layer in both the substrate and surface interfaces. Consequently, the film boundary conditions have strong influence in the orientation of the microdomains in the film. Bulk domain morphologies will generally be broken at the interfaces confining the film. The situation becomes even more involved when defects and non-equilibrium structures have to be taken into account. [48-50]

Preferential wetting occurs to minimise the free energy and the wetting of either the air or substrate interfaces by one block leads to a parallel orientation of the microdomain with respect to these interfaces. [51] For films having thicknesses less than the characteristic period, interfacial interactions will dictate the wetting layers at the interfaces, but the film thickness constraints may result in a change in the fundamental repeat of the morphology or a change in the morphology itself. [49, 52]

Symmetric boundary conditions can be realized when films are sandwiched between two substrates. In the studies, hard boundaries e.g. glassy polymers or evaporated SiO_2 introduced to the system were strongly attractive to one of the copolymer blocks, a condition that greatly stabilises surface parallel morphologies. If the films are confined between parallel walls and have strong interactions with either block, the frustration imposed by an incommensurate film thickness cannot be relieved by the island and hole formation. Instead the repeat period is altered and the copolymer chains stretch or compress in response to the constraint and the films show different periods in these films than in bulk or in pseudo-confined (on a substrate) films. [53, 54]

Asymmetric boundary conditions are the case for such films that are cast on a substrate. They form the majority of technologically relevant and experimentally tractable specimens. Asymmetry in block copolymer composition results in interesting phenomena for thin film morphology when compared to symmetric cases. This is easy to envisage if considered the case where the minority component wants to preferentially enrich the substrate surface. Even if the surface-enriching block is present in the

minority phase, a continuous wetting layer of that phase can still be present at the surface. Such a wetting layer can alter the near surface morphology. [53, 55]

4.2 Formation of Islands and Holes

In the case of symmetric diblock $(\varphi_A = \varphi_B = 0.5)$ copolymers, lamellar microdomains of thickness L_0 are formed. They can be aligned parallel to the plane of the film by boundary effects. When both boundary surfaces attract the same block, film thickness equals an integer multiple of L_0 and results in stable, flat films. Deviations from the quantised thicknesses will lead to self-dewetting and the formation of islands and holes in the free surface of the film. [56, 57]

The component with the lower surface energy typically resides at the free surface. If the other component resides at the substrate then the lamellae generally orient normal to the substrate. The topography of these ordered films is determined by the commensurability between the local film thickness and the interlamellar spacing. The local film thickness is $h = H_n = (n + \frac{1}{2})L$, where n is an integer. Islands, holes and bicontinuous patterns form when the thickness deviates by an amount $\Delta h > 0$ ($h = H + \Delta h$). In Figure 14 can be seen different topographical features. [17, 57]

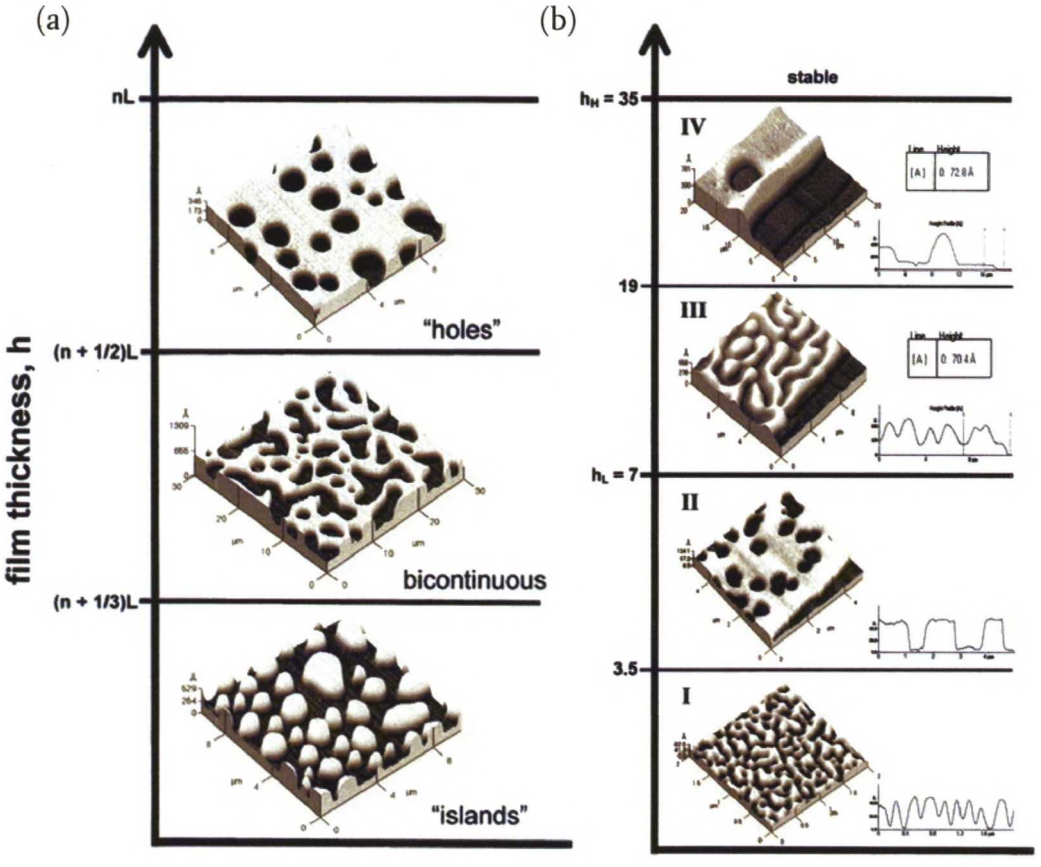

Figure 14. (a) AFM images of topographical features that appear in symmetrical PS-*b*-PMMA thin films on SiO_x surface. (b) Topographical features and pattern formation versus film thickness. [57]

Two distinct mechanisms of evolution and coarsening of islands and holes from the as-cast state are observed. [58-60] In one case the islands slowly nucleate and grow, while the other mechanism is characterized by a spontaneous evolution of surface structure followed by rapid coarsening. [58] Both mechanisms and the development upon aging time can be seen in Figure 15, where the evolution of films of diblock copolymer of poly-vinyl-cyclohexane (PVCH) and poly-ethyleneoxide (PEE) can be seen over time.

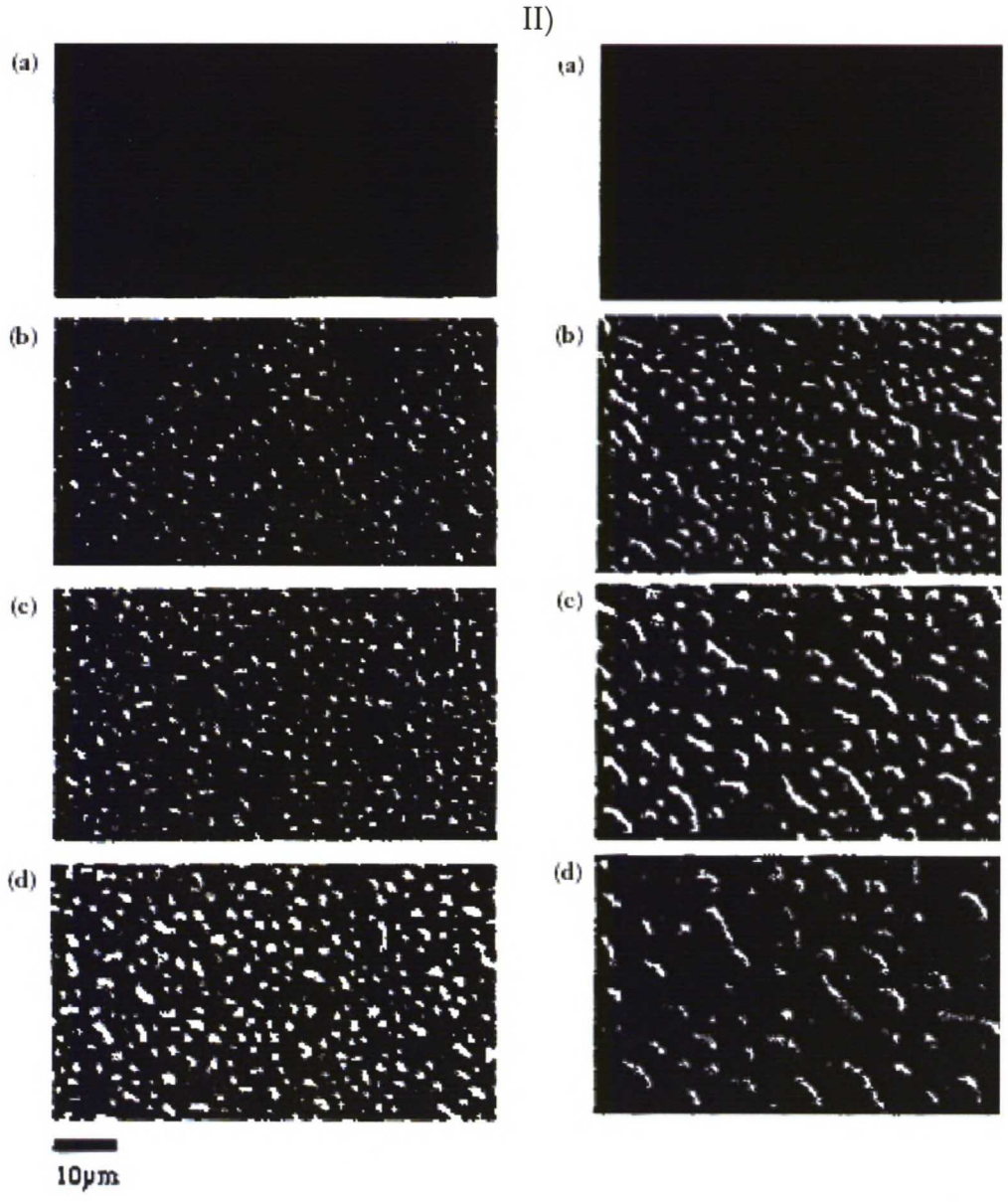

Figure 15. Optical microscope pictures of PVCH-PEE film as a function of time. I) Evolution of surface topography by nucleation and growth on the surface film when the temperature is increased to 190 C a) as cast; b) 40 s; c) 226 s; d) 7 min 20 s. II) Evolution of surface topography by a spontaneous transition on the surface of the film when the temperature is increased to 220 C a) as-cast; b) 30 s; c) 90 s and d) 210 s. [58]

5 TECHNIQUES FOR STUDYING BLOCK COPOLYMER THIN FILM STRUCTURES

5.1 Atomic Force Microscopy

5.1.1 Introduction to AFM

The Atomic Force Microscope (AFM), sometimes also called Scanning Force Microscope, belongs to a family of Scanning Probe Microscopes used for studying surface properties of materials from atomic to micron level. Typical AFM instrument can be seen Figure 16. [61, 62]

Figure 16. Digital Instrument MultiMode AFM equipped with the atmospheric hood. [63]

In atomic force microscopy the surface is probed with a sharp probe and interaction or interactions between the tip and the sample are monitored. The tip is a couple of micrometers long and often around 100 Å in diameter and the tip is located at the free end of the cantilever, which is 100 to 200 μm long. Forces between the tip and the sample surface cause the cantilever to bend or deflect. The measured cantilever deflections allow computer to generate a map of the surface topography. Sample is

placed on a piezoelectric scanner, which moves the sample under the tip (or in some cases, tip over the sample) in a raster pattern. Scanner is made of piezoelectric material, which expands or contracts proportionally to an applied voltage. To the scanner, there is a computer system attached that measures the data and converts it into an image. [61, 62] Sample operating environment can be ambient air, liquid, or vacuum. Resolution can be up to 2 nm in (x,y)-directions and 0.1 nm in (z)-direction. Total magnification can be up to 10^8. [63]

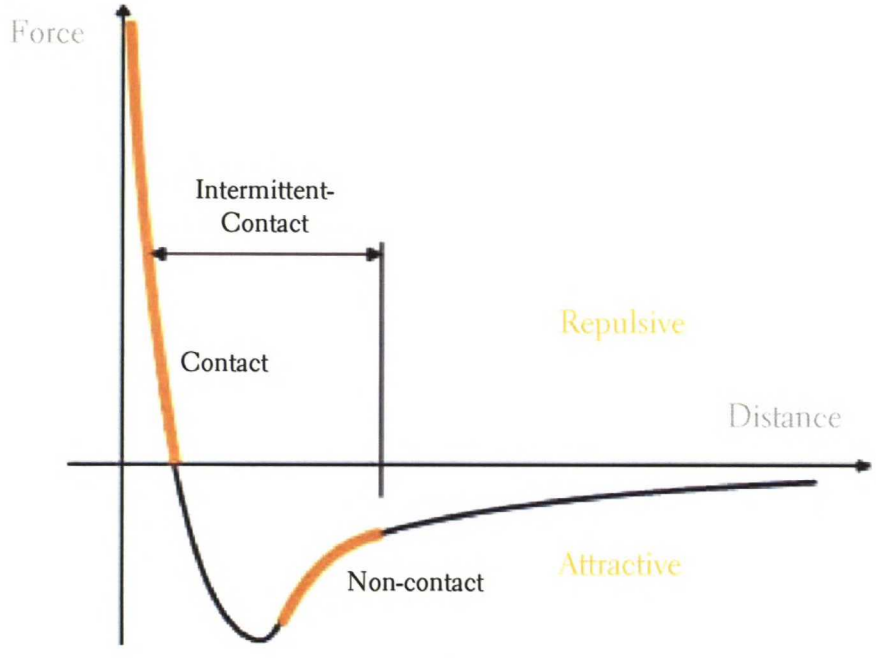

Figure 17. Force versus distance –curve with different operating modes of AFM: non-contact, contact and intermittent-contact modes. [61]

The tip operates in the near field, where it is affected by the van der Waals forces. On the right hand side of the Figure 17, atoms are separated by a large distance. As they are gradually brought together, they first weakly attract each other. This attraction increases until the atoms are so close that their electron clouds begin to repel each other electrostatistically.

The two distance regimes in the Figure 17 are labelled according to the operating mode; the intermittent mode penetrates into both of the regimes. The slope of the van der Waals curve is quite steep in the contact regime. In AFM this means that when the cantilever pushes against the sample, the cantilever bends rather than forces the tip atoms closer to the sample atoms. [61]

5.1.2 *Different AFM Operating Modes*

Atomic Force Microscopy can be operated on several different modes: contact mode, non-contact mode, and TappingMode™ also known as intermittent contact mode. TappingMode™ is a registered trademark of Digital Instruments. [62]

Contact mode, also known as the repulsive mode, operates by scanning the cantilever deflection with a split photodiode detector. The tip makes a soft physical contact with the surface through the absorbed fluid layer on the sample surface. A feedback loop maintains a constant deflection between the cantilever and the sample by vertically moving the scanner at each (x,y) data point. Computer stores the distance the scanner moves at each point. A topographic image is formed from the data. [61, 62]

In addition to van der Waals forces, two other forces are generally present during the contact-AFM: capillary force exerted by the thin layer of water present in an ambient atmosphere, and the force exerted by the cantilever itself. [62]

In the non-contact regime, the AFM is operated by scanning a tip, which is attached to the end of an oscillating cantilever. Cantilever is oscillated at a frequency slightly above cantilevers resonance frequency. In non-contact mode the tip does not contact the sample surface, but oscillates above the absorbed fluid layer on the surface during scanning. The spacing between the tip and the sample is on the order of tens to hundreds of ångströms. [62]

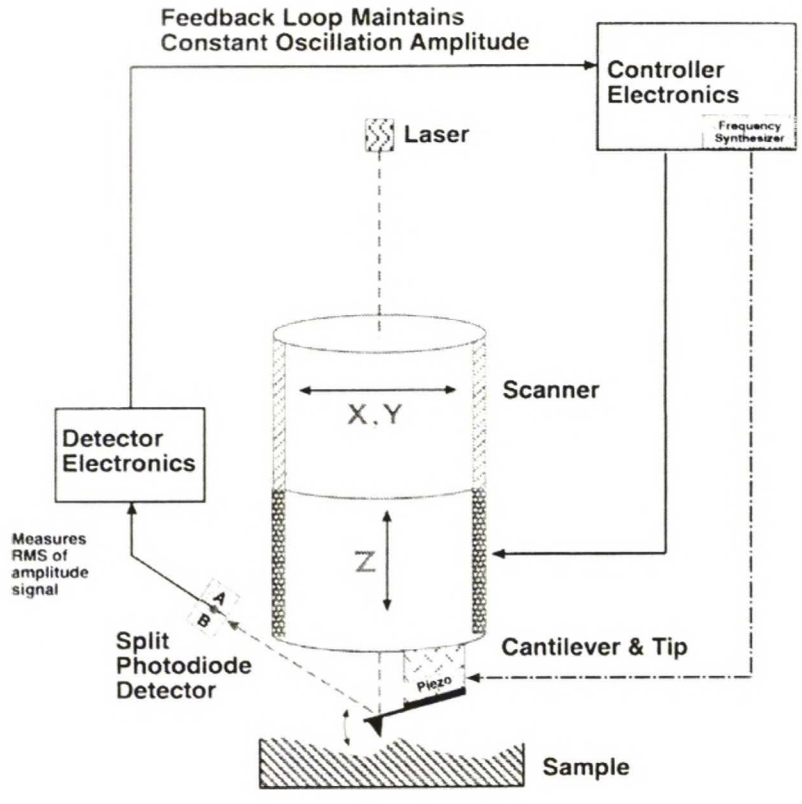

Figure 18. Typical component set-up for TappingMode™ measurements consists of scanner with cantilever attached to it, detector and the feedback loop. [62]

In the TappingMode™ -set-up (in Figure 18) the tip is attached as described above, but the cantilever is oscillated at its resonance frequency. The tip slightly "taps" on the sample surface, contacting the surface at the bottom of the swing. The feedback loop maintains constant oscillation amplitude by maintaining a constant root-mean-square of the oscillation signal acquired by the split photodiode detector. This way the tip-sample interaction is kept constant during imaging. Operation can take place in ambient and liquid environments. [62]

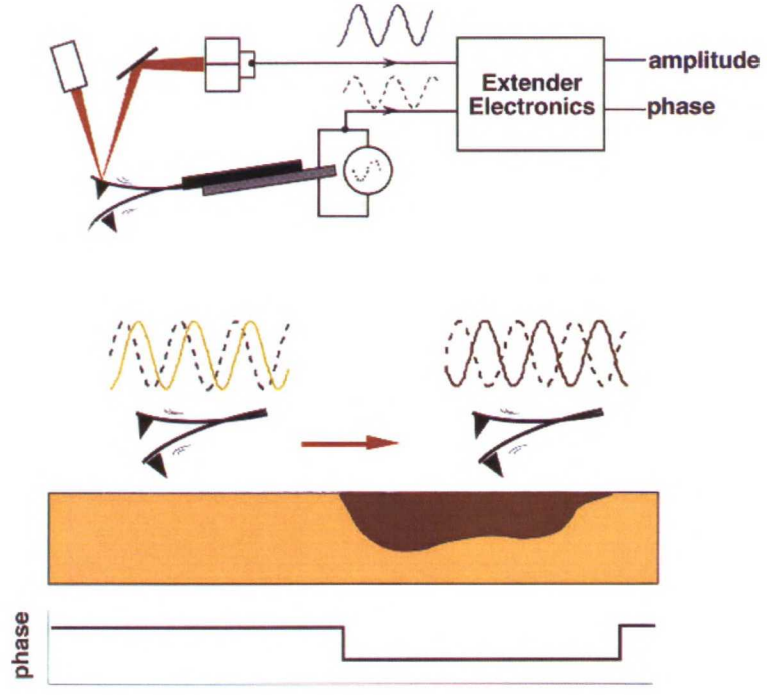

Figure 19. The phase lag of the cantilever oscillation (solid wave) can be seen in relation to the piezo drive (dashed). Spatial variations cause shifts in the cantilever phase and the phase image is produced by mapping the variations (bottom). [64]

In order to get information besides the topography of the sample, the phase lag of the cantilever oscillation can be investigated. This brings additional information about composition, adhesion, friction, and viscoelasticity. The phase lag is measured by the lag of cantilever oscillation to the piezo drive. Spatial variations in sample properties cause shift in the cantilever phase and can be mapped to produce the phase image as seen in Figure 19. [64]

5.2 Scanning Electron Microscopy

5.2.1 Introduction to SEM

The electron microscope can be defined as a device, which uses electrons to obtain magnified image of the specimen. In the family of electron microscopes, the Scanning Electron Microscope (SEM) constitutes one of the older and one of the most widely used instruments for surface analysis.

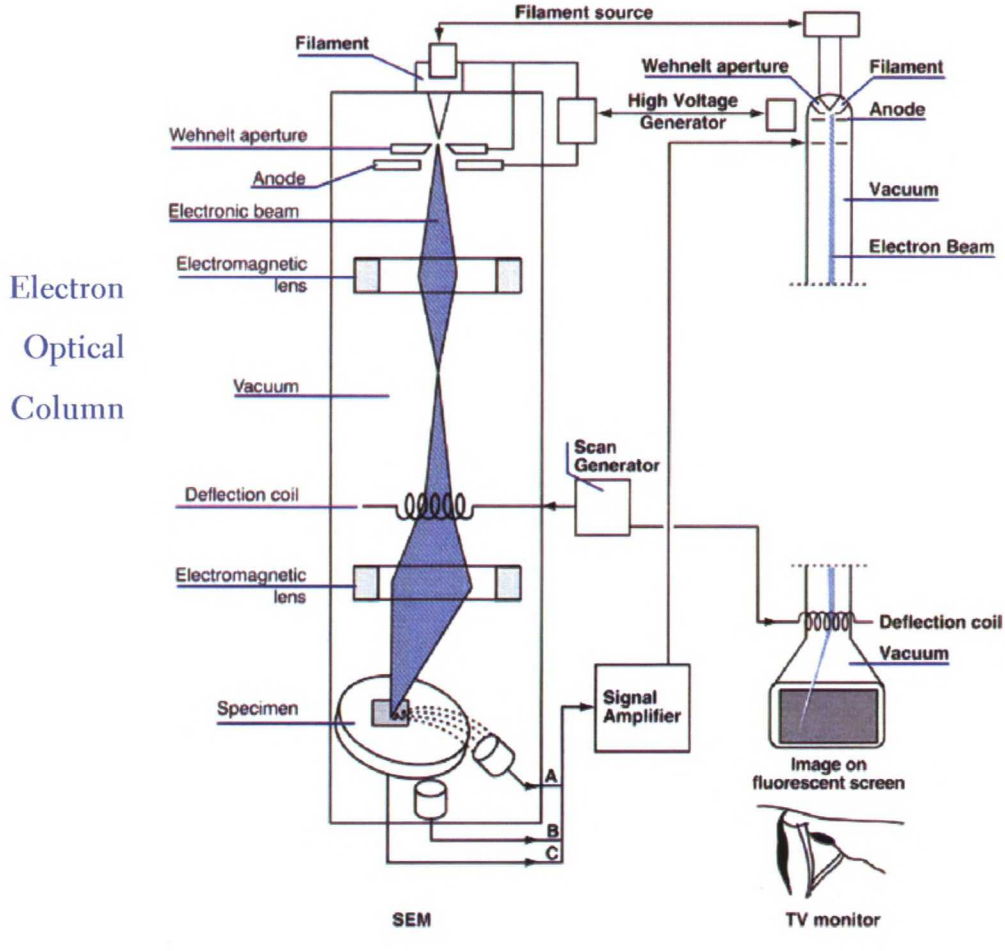

Figure 20. Scanning Electron Microscope (SEM) system consists of electron source, column, lenses, vacuum system and electronics. [65]

The SEM-system consists (Figure 20) of an electron optical column, a vacuum system, and the electronics. At the top of the column, the electron gun produces an electron

beam. There are three types of electron guns, a conventional triode electron gun, LaB_6, and field emission gun. The accelerating voltages in a SEM range from 200 to 30 000 volts. The electron beam is focused on the specimen through lenses. The condenser and objective lens systems are used to demagnify the electron beam formed at the crossover in the electron gun to the final spot on the sample. Beam magnification is needed because the beam diameter produced directly by the electron gun is too large to generate a sharp picture at high magnification. Column has three lenses, the final lens focuses the beam onto the surface of the specimen and the beam is scanned in a rectangular raster over an extremely small area. Beam is scanned over the specimen and secondary (or back-scattered) electrons are produced on the surface layer. Signal goes to a suitable detector, is amplified and used to modify the brightness of the cathode ray tube (CRT), which scans in synchronism with the primary beam. [65-70]

Detectors for secondary and backscattered electrons are usually either a scintillation detector or a solid-state detector. In the former case, electrons strike a fluorescent screen, which thereupon emits light; signal is amplified and converted into an electric signal by photomultiplier tube. The latter works by amplifying minute signal produced by the incoming electrons in a semiconductor device. [65]

5.2.2 *Imaging and Sample Preparation*

It was shown by Rayleigh that the maximum resolving power of any microscope is approximately λ, where λ is the wavelength of the radiation. In the case of the visible light the value of λ is about 500 nm. It was later shown by de Broglie that electrons can be considered as waves and the wavelength can be written as $12.5/V^{\frac{1}{2}}$ Å, where V is the accelerating voltage. For example, at 100 kV the wavelength is about 0.004 nm. [66, 70]

In principle, the resolution is determined by the electron beam diameter. The practical resolution however depends on the properties of the specimen and its preparation technique. In addition to that, many instrumental parameters affect the final resolution such as beam intensity, accelerating voltage, scanning speed, distance from the last lens to the specimen (working distance), and the angle between the specimen surface and the detector. [65, 71]

Advancements in the SEM technology have significantly increased resolution. Technological improvements have been optimised to allow SEM operation at low accelerating voltages. Low-voltage SEM (0.5-5.0 keV) of polymers is advantageous over conventional SEM (10-35 keV) due to the reduced amount of charging artefacts and significantly improved topographic contrast. Technological enhancements include the field emission source for the electron beam, a high excitation, short-focal-length lens, and a better vacuum. The downside is that the field emission gun requires a higher vacuum and in some cases the primary beam damages the specimen surface very quickly. [72, 73]

The ratio between the size of the screen of the viewing monitor and the size of the area scanned on the specimen is the magnification. The data is recorded by photographing the monitor screen. [65, 69] Under optimum conditions in low-voltage scanning electron microscope a resolution of 1 nm can currently be attained. [71]

SEM can be used whenever information is required about the surface of the specimen or by increasing the acceleration voltage, a layer of several micrometers can be studied. The only requirement is that the sample can withstand the vacuum and the electron bombardment. [65]

In polymer samples the combination of low atomic number and low density results in poor electron scattering and gives low contrast. Staining enhances contrast. Specimen is exposed to the vapour of the staining substance. Materials used for staining can be e.g. OsO_4 or Iodide. The osmium tetraoxide selectively stains the carbon-carbon double bonds. [74]

Most polymers are insulators; the non-conducting nature causes both charge and thermal build-up when bombarded with electrons. Charging in polymers necessitates coating samples with a conductive metal film in conventional SEM imaging. Thick coatings of gold, gold-palladium, or platinum-palladium are either sputtered or evaporated onto the sample. Carbon is also sometimes used. The coatings are thicker, typical thickness of 100-200 Å, than the secondary electron escape depth for metals at the low voltage. [72]

II EXPERIMENTAL PART

6 AIM OF THE STUDY

The main object for the experimental part was to investigate self-organised structures of block copolymers and formation of block copolymer/amphiphile supramolecules in thin films and launch extensive study of block copolymer thin films in the laboratory of Optics and Molecular Materials at the Helsinki University of Technology.

Thin films were spin-coated on silicon or polyimide substrates. In this work poly(styrene)-*block*-poly(methyl methacrylate) (PS-*b*-PMMA) and poly(styrene)-*block*-poly-(4-vinyl pyridine) (PS-*b*-P4VP) were used. The compositions were selected so that in bulk the minority block microphase-separates to form a cylindrical phase and the major block forms the matrix surrounding the cylinders (see Figure 7b and d). In the case of PS-*b*-PMMA two different compositions were examined with either PS or PMMA as the matrix component. In the case of PS-*b*-P4VP the polymer was first studied as such and additionally an alkyl tail was added to study the block copolymer/amphiphile interaction in thin films. Pentadecylphenol, an alkylphenol with 15 methyl units, was added in order to manufacture thin films with so-called structure-within-structure morphology. In bulk several hierarchical morphologies can be seen, such as lamellar-within-lamellar and lamellar-within-cylinder structures. [18, 75]

Spin-coated films are not typically equilibrium structures due to the fast solvent evaporation and annealing is needed to allow more global order with uniform alignment of the local self-organised structures. Different annealing methods were considered from the literature and thermal annealing and solvent swelling were selected. Thermal annealing was performed in temperature 40 degrees above block copolymer's highest glass transition temperature. In polymer swelling experiments the thin films were exposed to a controlled partial pressure of chloroform. The resulting microdomain structures were quenched via fast solvent removal.

Thin films were studied using AFM and field emission scanning electron microscope (FE-SEM).

In the experiments PS-*b*-PMMA was found to form worm-like cylinders and spheres. Studied films' thickness was less than one repeat distance thick i.e. they are called ultrathin films. Reverting the matrix component from PS to PMMA caused no change in the morphology. Substantially longer annealing times and tuning the thickness closer to one repeat thickness would no doubt produce better films. In solvent annealing method a PS layer was observed to be the top layer. It appears that solvent annealing is superior over thermal annealing as a method and equilibrium or near-equilibrium structures are obtained much quicker.

Secondly thin films were manufactured with material that allow structural hierarchy upon introducing. PS-*b*-P4VP thin films were studied with AFM but the method proved to show nothing conclusive. The film morphology was measured with SEM and the structure was observed to be parallel to the substrate. The morphology of the thin film was the same as in bulk and the level ordering depends on the contact time with the solvent.

PS-*b*-P4VP was introduced with pentadecylphenol (PDP) to form hierarchical structures. The expected bulk structure of lamellar-within-cylindrical was not observed. Three possible explanations are given, the most probable being the side-chain crystallisation that forces the structure to be lamellar-within-lamellar. The more unlikely explanations are that a non-hierarchical lamellar structure is formed, either because the PDP has left the structure or the surface effects demand a lamellar morphology.

7 MATERIALS

7.1 Poly(styrene)-*block*-poly(methyl methacrylate)

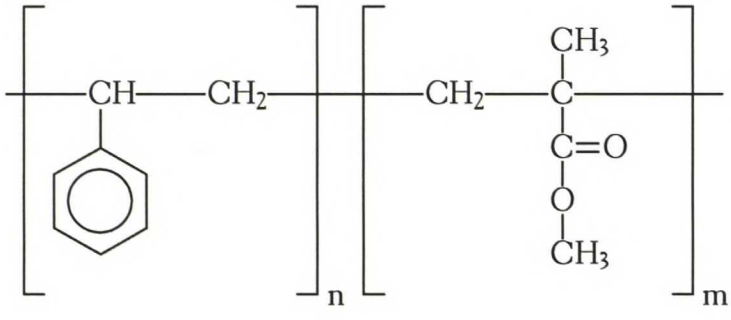

Figure 21. PS-*b*-PMMA. Block copolymer consists of a poly(styrene) (PS) block with *m* repeat units and a poly(methyl methacrylate) (PMMA) block with *n* repeat units. See Table 1 for repeat units and other specifications used in the experiments.

Diblock copolymer PS-*b*-PMMA was chosen as the starting material due to the extensive research and information available on the material by several research groups. [35, 76-80] PS-*b*-PMMA (Figure 21) has interesting applications, because the PMMA can be degraded away by UV-radiation, thus allowing e.g. nanoscale structuring of photoresist materials for electronics. Especially interesting are the compositions where the w-% of PMMA ranges from 16 to 32 w-% and PMMA is theoretically expected to form microphase-separated cylinders. [81] Cylinders can be aligned perpendicular to the substrate with methods described in Chapter 3.5. Ideally these upright cylinders are arranged in hexagonal packing. [35] Degradation of globally aligned cylinders leaves the thin film with nano-sized empty cylinders whose size can be tuned by the choice of the block lengths. This new material might also have a use in fuel cell technology, drug transportation or as a nano-sized sieve.

Another reason to choose this material as a starting point was due to the known behaviour to have sufficient contrast between the two phases in AFM phase

measurements. Both blocks of PS-*b*-PMMA are glassy in ambient atmosphere, but the relative hardnesses of the phases differ sufficiently.

Two different compositions of PS-*b*-PMMA were acquired from Polymer Source Inc. (Canada) and used without further purification. Theoretical bulk morphologies of the block copolymers obtained are cylindrical i.e. the minority block is microphase-separated into shape of cylinders. One of the polymers has PMMA as the cylinder phase and another one has PS as the cylinder phase. In Table 1 are listed the block lengths, weight percents, polydispersity M_w/M_n (PD), the amount of repeat units, and the morphology of the polymers used.

Table 1. Properties of PS-*b*-PMMA polymers used in the experiments.

Polymer no. #	PS-block (*g/mol*) / Repeat units *n*	PMMA-block (*g/mol*) / Repeat units *m*	PS (w-%)	PD	Bulk morphology
P717	96 300 / 920	35 500 / 350	73	1.11	PMMA Cylinders
P718	45 900 / 440	138 000 / 1380	25	1.16	PS Cylinders

7.2 Poly(styrene)-*block*-poly(4-vinyl pyridine)

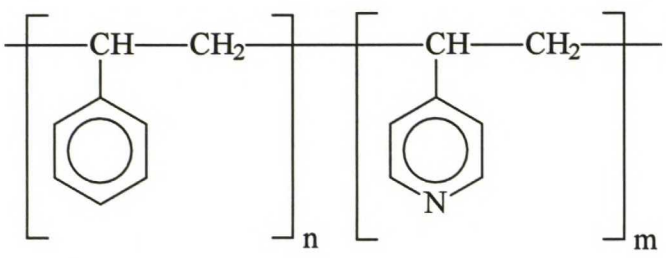

Figure 22. PS-*b*-P4VP. Block copolymer consists of poly(styrene) block with *n* repeat units and poly-(4-vinyl pyridine) block with *m* repeat units. For the polymers used, specifications are listed in Table 2. Blocks are relatively similar and the positioning of the nitrogen atom enables the addition of hydrogen-bonded material.

Poly(styrene)-*b*-poly(4-vinyl pyridine) (PS-P4VP) was studied as it allows structural hierarchy upon introducing. As seen in Figure 22, P4VP and PS are relatively similar polymers. Until recently PS-*b*-P4VP has been quite rarely used as a block copolymer material due to the difficult synthesis, whereas poly(styrene)-*b*-poly(2-vinyl pyridine) (PS-*b*-P2VP) has been widely employed to provide polymer brushes on polar surfaces. Recently these spatially functionalised polymers, so-called polymer brushes, have increasingly become a focus in biology and medicine. Generation of specific patterns on a substrate offers the ability to direct important interfacial phenomena such as wetting, fluid flow, and adhesion. PS-*b*-P4VP is a related material to PS-*b*-P2VP, but provides better possibilities for hydrogen bonding due to the better positioning of nitrogen atom in the heteroaromatic ring. [82]

Several different compositions of diblock copolymer were used. Polymers were acquired from Polymer Source Inc. (Canada) and used without further purification. In the polymers used, the P4VP was the minority block, usually weight fraction corresponding to cylinder morphology in bulk. Specifications of the polymers used like poly(styrene) weight percents, block lengths, repeat unit amounts, polydispersity, and morphology are listed in Table 2.

Table 2. Properties of PS-*b*-P4VP polymers used.

Polymer no. #	PS-block (*g/mol*) / Repeat units *n*	P4VP-block (*g/mol*) / Repeat units *m*	PS (w-%)	PD	Bulk morphology
P99	32 900 / 320	8 000 / 80	80	1.06	P4VP Cylinder
P112	18 600 / 180	55 800 / 530	25	1.26	P4VP Cylinder
P141	42 100 / 400	8 100 / 80	84	1.08	P4VP Cylinder

7.3 Poly(styrene)-*block*-poly(4-vinyl pyridine)·(pentadecylphenol)$_{1.0}$

The pure diblock polymer PS-*b*-P4VP is self-organised in nanoscale and the measure of the structural size is called the long period. Long period means the distance from begin of the periodic structure to the starting point of next period. For example, in PS-*b*-P4VP the lamellar structure long period could be defined from the beginning of PS lamella to

the end of P4VP lamella in a perpendicular direction. For cylinders the long period would be from the centre of the cylinder to the centre of the adjacent cylinder. In diblock copolymers the long period is typically around 10-100 nm.

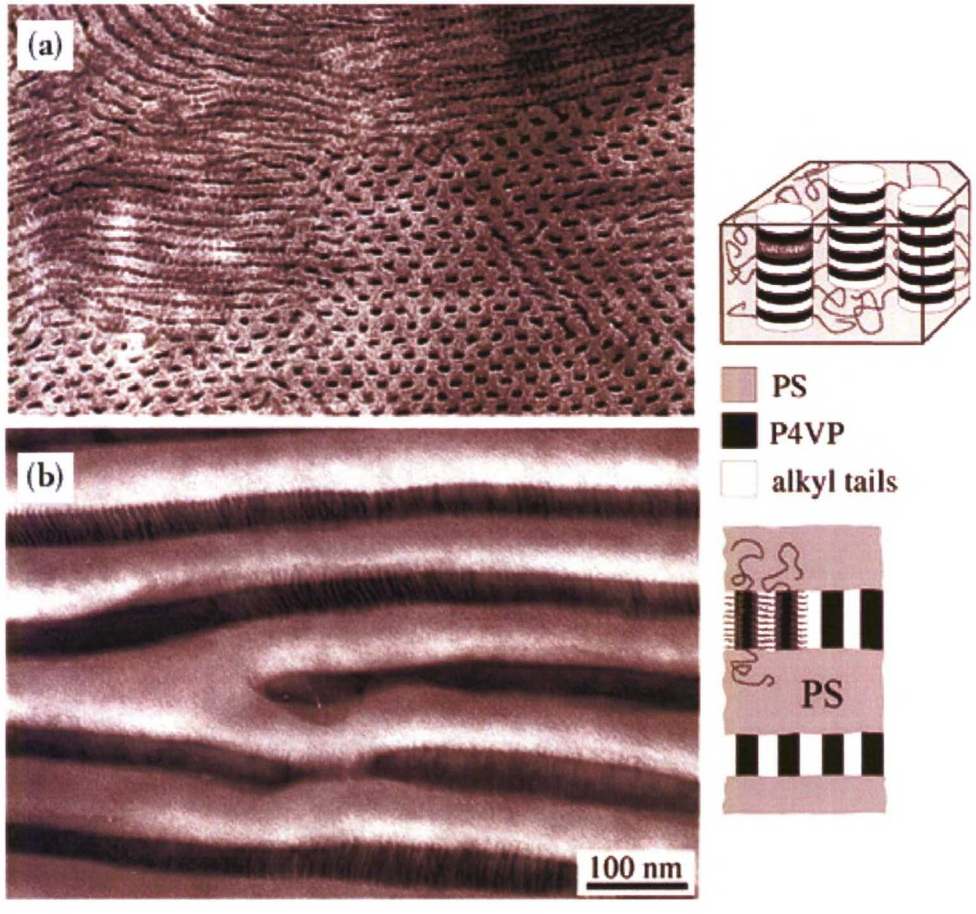

Figure 23. Typical examples of bulk morphologies with structures-in-structures shown by TEM. Polymer is PS-*b*-P4VP with nonadecylphenol (NDP), alkyl tail with 19 methyl units. Morphologies are: (a) Lamellar-within-cylinder, where inside poly(styrene) matrix are cylinders with the lamellar structure consisting of P4VP and NDP. (b) Lamellar-within-lamellar, where poly(styrene) forms the other lamellae phase and the other phase consists of lamellar structure of P4VP and NDP.

The addition of amphiphiles introduces another length scale to the structure. These hierarchical structures combine the block copolymer nanostructures with one order of magnitude smaller length-scale organisation within one of the microphase-separated domains either using covalently bonded mesogenic moieties or using mesomorphic

polymer/amphiphile complexes for one block. Typical length scale is 2-6 nm. Ruokolainen *et al.* [18, 75] have demonstrated that one can obtain lamellar-within-lamellar, lamellar-within-cylindrical, cylindrical-within-lamellar, spherical-within-lamellar, and spherical-within-lamellar morphologies. Examples of this supramolecular self-organisation are seen in Figure 23.

In this work an amphiphile, pentadecylphenol (PDP), was added to the PS-*b*-P4VP polymers to tune the effective weight fraction of the P4VP fraction (Figure 24) from spherical to hierarchical lamellar-within-cylindrical. Motivation was to study how the corresponding hierarchical structures in thin film differ from the bulk structures mentioned in the previous chapter (see also Figure 23). Another motivation that suggested attempting experiments with this material was the identification of an alternative annealing method i.e. solvent annealing. Previously annealing has caused troubles, because PDP becomes miscible in PS phase above about 130 °C. [83] Thermal annealing has to be performed temperatures higher than the highest glass transition temperature of the blocks. Highest T_G without PDP would be that of P4VP block (146 °C), but as PDP plasticises the P4VP phase in the amphiphile mixtures, the highest T_G is that of the PS phase (100 °C). Required annealing temperature is too high for the hierarchical structure and other methods have to be used instead.

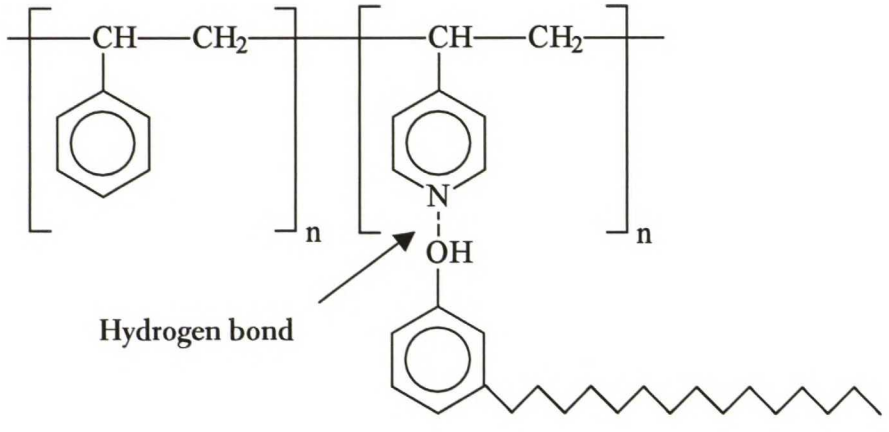

Figure 24. PS-*b*-P4VP(PDP)$_{1.0}$. Block copolymer consists of poly(styrene) block with m repeat units and poly(4-vinyl pyridine) block with n repeat units. Polymer compositions are listed in Table 3. For every 4-vinyl pyridine moiety there is nominally one pentadecylphenol molecule attached by a hydrogen bond.

PDP consists of phenol with an alkyl tail of fifteen methyl units. The addition of PDP increases the volume fraction of the P4VP phase by supramolecule formation. Theoretically and in bulk this addition would tune the morphology from spherical to lamellar-within-cylindrical hierarchical structure.

As an example, let's consider a bulk sample of polymer #P135, where the block lengths are 34000 g/mol for the PS block and 2900 g/mol for the P4VP block, i.e. the number of repeat units is respectively 330 and 30. To add an equivalent amount of one PDP molecule per one P4VP repeat unit, 30 molecules of PDP per P4VP block is needed. Knowing the molecular weight of PDP and the amount of polymer used, we can add nominally stoichiometric amount of PDP. Table 3 shows the compositions.

Table 3. Properties of PS-*b*-P4VP(PDP)$_{1.0}$ polymers used.

Polymer No. #	PS-block (*g/mol*) / Repeat units *n*	P4VP-block (*g/mol*) / Repeat units *m*	PS (w-%)	PD	PDP per 1 g of polymer (g)	Bulk morphology
P98	35 500 / 340	3 600 / 30	91	1.06	0.27	P4VP Sphere
P135	34 000 / 330	2 900 / 30	92	1.07	0.23	P4VP Sphere

PDP used in the experiments was 98% (Aldrich) pure and it was purified by recrystallisation from petrol ether. Nominal amount of PDP was added for each P4VP repeat unit, but the actual number of PDP molecules hydrogen bonded to P4VP is uncertain. Based on previous studies by Fourier-Transform Infrared Spectroscopy it is expected that the equilibrium constant is overwhelmingly in favour of hydrogen bonding. [85] PDP was added for two copolymer systems of PS-*b*-P4VP. The morphology of these polymers was that P4VP was the minority phase with a spherical morphology. The polymers used were #P98 and #P135, further specifications can be seen in Table 3.

7.4 Solvents

Toluene C_7H_8, in Figure 25a, also known as phenyl methane or methyl-Benzene, was used as a solvent for the PS-*b*-PMMA thin films. Purity grade was 99.96% (Fischer). The molecular weight of toluene is 92.1 $\frac{g}{mol}$ and boiling point 110.6 °C.

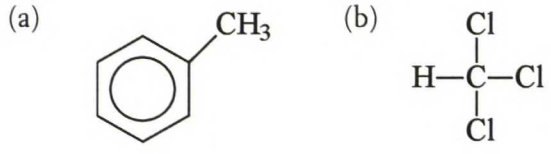

Figure 25. The structures of solvents used: (a) toluene, (b) chloroform.

Chloroform $CHCl_3$, in Figure 25b, also known as trichloromethane, was used as a solvent for the preparation of PS-*b*-P4VP and PS-*b*-P4VP(PDP)$_{1.0}$ thin films. Solvent's purity grade was 99.0% (Riedel-de Haën). The molecular weight of chloroform is 119.4 $\frac{g}{mol}$ and boiling point 61.7 °C.

7.5 Substrates

In thin films where the film thickness is far less than the lateral extent of domains the quality and flatness of the substrate plays a significant role. The size of the domains is usually around 1 μm and typical film thickness is from 30 nm to couple of hundreds of nanometers. The substrate-film interface demands that the most energetically compatible block is located on the surface. Polar surfaces like silicon attract the more polar block and the in the present cases the PMMA or P4VP blocks. In the film-air interface the less polar is block is preferred, in this case it's PS. The wetting of the surface depends mainly on the magnitude and type of interactions these boundaries have with each of the block species.

Silicon is extensively used as a substrate material to prepare thin films due to the inert nature and flatness of the substrate. The top layer is flat all the way down to the atomic level and therefore it is a very suitable for thin and ultra-thin films. Silicon wafers are

anisotropic. The crystalline directions of interest include the <100>, the <110>, and the <111> crystal directions. Silicon used in these experiments were of crystalline direction <100>, since silicon breaks up easily along <111> cleavage planes and therefore the large round wafer is easy to cut in to smaller rectangular pieces required by the AFM specimen discs.

Silicon wafers were used as purchased (Silicon Quest International) except for a rinse in acetone prior to spin-coating to remove the airborne contaminants. The wafers' thickness was 13-17 mm and had a layer of native oxide layer approximately 1-2 nm thick.

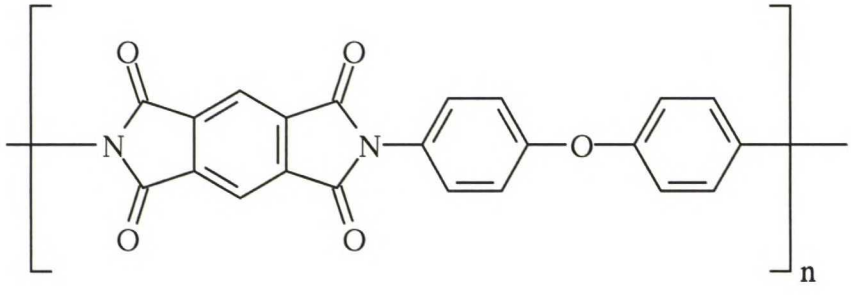

Figure 26. The chemical structure of Kapton®-type poly(imide) contains several polar atoms like oxygen. Due to the nature of the chain, poly(imide) is also very inert chemically and has excellent physical, mechanical and electrical properties. The problem is that commercially produced films are not very flat.

On the other hand, poly(imide) (Figure 26) was chosen as the other substrate due to its chemical inertness. Poly(imide) is a polar substrate with excellent chemical resistance and there are no known organic solvents for the film. Poly(imide) maintains also its physical, electrical, and mechanical properties over a wide temperature range. Advantage over silicon is that with poly(imide) substrate Small-Angle X-Ray Scattering measurements can be performed. Disadvantages are the relative roughness of the film and the flexibility of the substrate. Even very slight deformation of the flexible substrates may destroy the structure. The film surface was measured with AFM and the surface had the average roughness of ±3 nm.

Poly(imide) (Kapton®) films were purchased from Du Pont (U.K.) Ltd and used in experiments as obtained except for a rinse in acetone to remove the airborne contaminants. The used substrate thickness was 50.8 μm.

Before spin-coating the substrates were cut to fit the AFM specimen discs (Ted Pella, Inc.) with the diameter of 15 mm. The size of the substrate used varied from 7 mm x 7 mm to 10 mm x 10 mm.

8 PROCEDURES

8.1 Atomic Force Microscopy

Atomic Force Microscope (AFM) measurements were carried out at The Helsinki University of Technology (HUT), Espoo, using NanoScope Multimode III microscope and at The Bayreuth University, Germany, using Digital Instruments NanoScope MultiMode III and Dimension 3100 Atomic Force Microscopes. All the measurements were performed in ambient atmosphere and when possible with damping to minimise the data artefacts caused by shocks or vibrations.

Several different types of silicon cantilevers were used with resonance frequencies between 290 and 330 kHz. The probes were operated in TappingMode™ and driven at 3-5% offset below their resonance frequencies. Topography and phase images were taken at scanning speeds of around 2-6 μm/s.

8.2 Scanning Electron Microscopy

Scanning Electron Microscopy (SEM) was used to study the morphology of the films when the contrast in AFM is not sufficient. In solvent annealing experiments a thin layer of PS resides on the polymer-air interface and therefore in AFM measurements nothing but homogenous film with no surface structure is seen. In PS-*b*-P4VP and in PS-*b*-PMMA systems, both blocks are glassy at room temperature. In PS-*b*-P4VP only topographical data provides information with AFM whereas PS-*b*-PMMA provides also phase contrast. This matter is not trivial and the true reason remains to be discovered.

SEM was performed in Bayreuth using LEO 1530 Gemini instrument equipped with a field emission cathode with a lateral resolution of approximately 2 nm. The acceleration voltage used was 0.68-8.86 kV. Prior to the measurements the films were stained with I_2 vapour for 3 hours to enhance the contrast between the phases.

9 SAMPLE PREPARATION

9.1 Spin-Coating

Spin-coating is a well-established method to prepare well-defined thin layers with smooth surfaces. The formation of layers relies on the rapid evaporation of the solvent. Thickness of the film can be tuned with two variables: spinning speed (revolutions per minute, rpm) and the solution concentration (grams of polymer per grams of solvent). Typical spinning speeds are from 500 to 8000 rpm. An increase in the spinning speed makes the films thinner. For polymers the typical solution concentration is 1-2 w-%. Increasing the concentration makes the film thicker.

Thin polymer films were prepared by spin-coating on silicon and poly(imide) substrates using spin-coater manufactured by Headway Research International: PS-*b*-PMMA polymers were spun from 1% toluene solutions and PS-*b*-P4VP with and without PDP were spun from 1% chloroform solution. 'These concentrations were chosen to be good average values found in the literature. Very dilute solutions tend to dewet and too concentrated solutions (> 2 w-%) produce thick films. The aim was to produce very thin layers where the effect of the surface is visible, because too thick a film behaves like a bulk sample.

For all the films the preferred solvent was expected to be toluene but only PS-*b*-PMMA films were soluble. Low boiling point solvents like chloroform tend to evaporate too quickly and leave the film too rough. Finding the right combination of spinning speed and solution concentration for low-boiling solvents is challenging.

Tuning of the film thickness was done mainly with the variation of the spinning speed. For toluene solutions the best spinning speed was found to be 1000-2000 rpm. With chloroform the suitable spinning speed varied between 2000 and 8000 rpm. High spinning speeds were used for solvent annealing method to observe structures with PS-*b*-P4VP$(PDP)_{1.0}$.

Additional samples of PS-*b*-P4VP(PDP)$_{1.0}$ were spun from 0.5% chloroform to obtain thinner films where dewetting was not observed except after very long annealing times in combination with high vapour pressures. The wetting and dewetting behaviour of the films is discussed in Chapter 10.

Film thicknesses were measured with AFM by applying a scratch to the film. A spin-coated and annealed sample was taken and a sharp object, usually a needle or scalpel, was used to mark the film with a scratch. Then the sample was taken to the AFM and the correct spot with the ridge was located on the film. An AFM image was taken and height difference between the substrate surface and the surface of the film was analysed from the data. This procedure is very useful with films on silicon substrate but applying a scratch to the film on the poly(imide) substrate cannot be performed without damaging the film or the substrate.

9.2 Annealing Methods

Two different annealing methods were used to monitor the effects of different preparing methods on the final morphologies of the films.

Thermal annealing was performed on temperatures well above block copolymers' glass-transition temperatures (T_G). Every block of the block copolymer has its own separate T_G, because the blocks are microphase-separated. Glass-transition temperatures of homopolymers PS, PMMA and P4VP are 100 °C, 105 °C, and 146 °C, respectively. Annealing has to be then performed at a higher temperature than the highest T_G of the blocks. Thermal annealing temperature was chosen both for PS-*b*-PMMA and PS-*b*-P4VP samples to be around 40 °C above the T_G to ensure sufficient mobility of the chains. For P4VP(PDP)$_{1.0}$ PDP plasticises the P4VP phase and it is known to become soluble in PS or phase separate in elevated temperatures so thermal annealing cannot be used with this material.

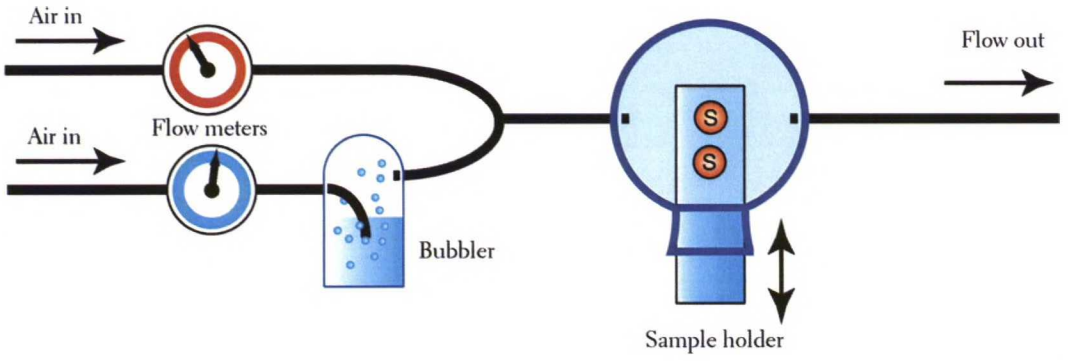

Figure 27. Experimental set-up for the solvent annealing experiments. Two lines of purified air flows in and one of them is bubbled through the liquid solvent phase with the solvent in the bubbler. The two lines are combined. The volume flows are known and the partial pressure can be calculated by assuming that the vapour in the solvent line is saturated. Air-solvent mixture flows to the sample chamber, fills the chamber and flows out at a controlled rate. Samples are quenched and current microstructure is frozen via fast solvent removal.

The alternative annealing method was studied at The Bayreuth University. The experimental set-up is as seen in Figure 27. Principle is to expose the thin films for several hours to a controlled partial pressure p of chloroform or other solvent vapour. Chloroform was used due to its low boiling point and relatively high volatility. The partial pressure, total pressure and the temperature were monitored. The resulting microdomain structures were quenched via fast solvent removal. During this solvent annealing, the non-selective solvent, $CHCl_3$, acts as a plasticiser to enhance the chain mobility and reduces time significantly for the structures to achieve equilibrium structures.

Spin-coated and annealed films were attached with the substrate to metallic AFM specimen discs with double-sided tape.

10 RESULTS AND DISCUSSION

Most of the data gathered for this thesis are pictures taken with Atomic Force Microscope. Typical AFM picture information consists of topographical data showing the height variations of the sample and phase data showing the relative hardnesses of the surface substances. In images presented in this thesis, a scale bar is added to visualise the relative sizes of the morphologies in hand. The colours used in the pictures are for visualisation purposes and have nothing to do with the colours of the actual samples. The same applies as in SEM images. Colours are purely for viewing purposes and do not represent the specimen colours.

10.1 Poly(styrene)-*block*-poly(methyl methacrylate)

Typical AFM image of PS-*b*-PMMA film of sample #P717 with expected morphology of PMMA cylinders in PS matrix can be seen in Figure 28. Topographical image offers us information about the surface structure and the topography of the composition. The PMMA cylinders are slightly protruded from the surface of the film but only about two nanometers. Also the film height itself varies slightly; the brown plateaus are about 2 nm lower than the yellow plateaus. The film thickness of the PS-*b*-PMMA samples was tuned by changing the spinning and was measured to be between 38 and 57 nm. The periodicity of the self-organised structure is roughly 60 nm, which makes the studied films' thickness less than one repeat distance thick i.e. ultrathin films.

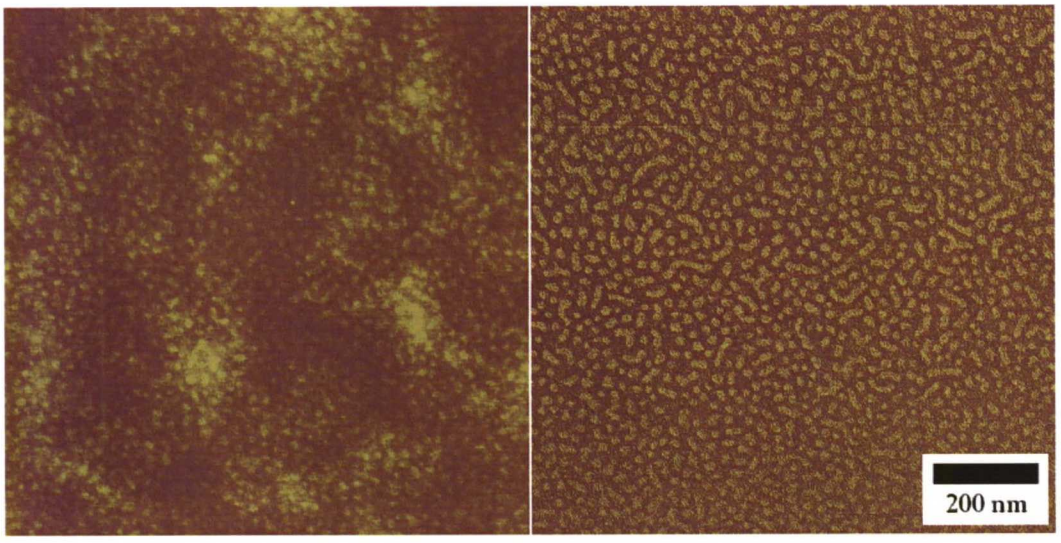

Figure 28. PS-*b*-PMMA film (thickness 42-46 nm) on the silicon substrate. The film was prepared from #P717 using 1 w-% toluene solution of polymer was spun with 2000 rpm. Film was thermally annealed at 140 °C for 72 h in vacuum ($2*10^{-1}$ mbar). The weight fraction of PS was 73 and therefore the expected morphology in bulk is PMMA cylinders in PS matrix. The AFM image was taken at HUT. In the topographical image (left) the height variation is 4nm. In the phase image (right) droplets and worm-like cylinders of PMMA (the yellow colour) parallel to the substrate can be seen.

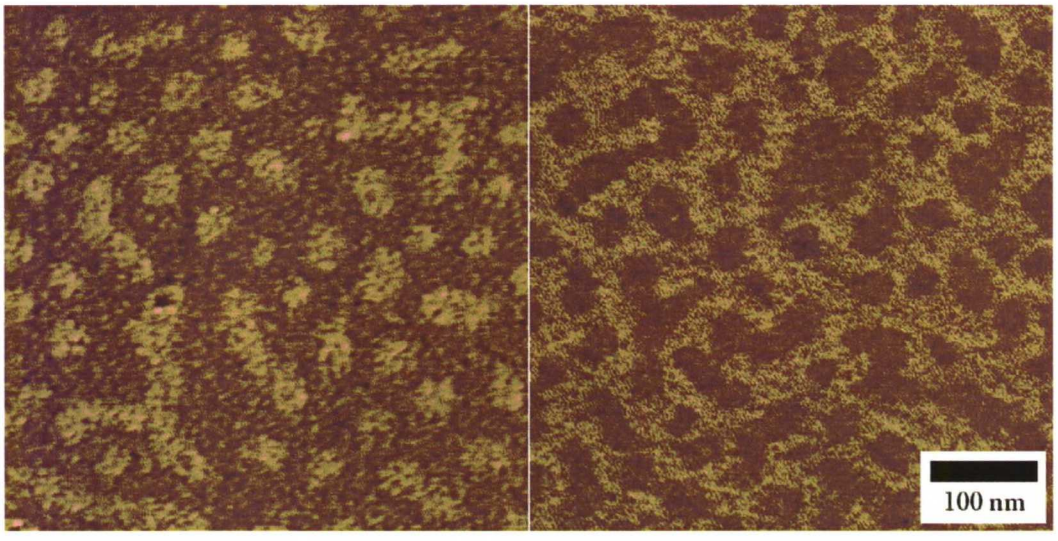

Figure 29. The phase images of PMMA cylinders in PS matrix (left) and PS cylinders in PMMA matrix (right) on a polyimide substrate. Samples are #P717 and #P718 prepared at HUT, 1 w-% toluene solutions spin-coated with 2000 rpm and annealed in 140 °C for 72 hrs in vacuum ($2*10^{-1}$ mbar). Film thicknesses were 42-52 nm. Worm-like cylinders and spheres are seen formed by the minor block: on the left PMMA (yellow), on the right PS (brown).

In Figure 29 there are two phase images of spin-coated samples on poly(imide) substrate: #P717 with the bulk structure of PMMA cylinders in PS matrix and #P718 with the bulk structure of PS cylinders in PMMA matrix. Reverting the matrix component from PS to PMMA seemed to cause no significant change in the morphology. The observations suggest that longer cylinders are in process to be formed and one could anticipate that after substantially longer annealing times than used in experiments, a worm-like structure would disappear and cylindrical morphology will form as seen in SEM picture in the following chapter. Problem with longer annealing times is the possible oxidation effect and that is why a ultrahigh vacuum is needed to minimise the effect of oxygen.

Figure 30. SEM image of a solvent annealed structure of PS-*b*-PMMA thin film of #P717 (thickness ca. 50 nm) measured with LEO 1530 Gemini FE-SEM. Sample was spin-coated to silicon substrate and annealed with solvent annealing for 6h in relative pressure of $p_{chloroform}$= 0,65. The expected structure in bulk consists of PMMA cylinders in PS matrix. Here we see PMMA cylinders (brighter blue) parallel to the substrate in PS matrix, which corresponds well to the bulk structure.

Figure 30 shows a Scanning Electron Microscope image of thin film annealed with solvent annealing set-up. The annealing produced cylinders parallel to the substrate. The annealing time turned out still not sufficient to orient the structures properly. One could speculate that with proper annealing in a non-selective solvent, the structures of PS-*b*-PMMA films would be a lot longer cylinders organized parallel to the substrate. The improvement to the thermal annealing is considerable and almost all evidence of the worm-like micelles and droplets or spheres has disappeared.

Typically it was observed that using thermal annealing the film surface morphology was independent of the substrate material and the film thickness when the film thickness is below one repeat distance. One could speculate that closer to a complete repeat thickness, better mobility of chains would be achieved and the top layer of PS becomes

possible. Longer annealing times would produce with no doubt similar structures as seen with solvent annealing. The proposed but unconfirmed structures are shown in Figure 31.

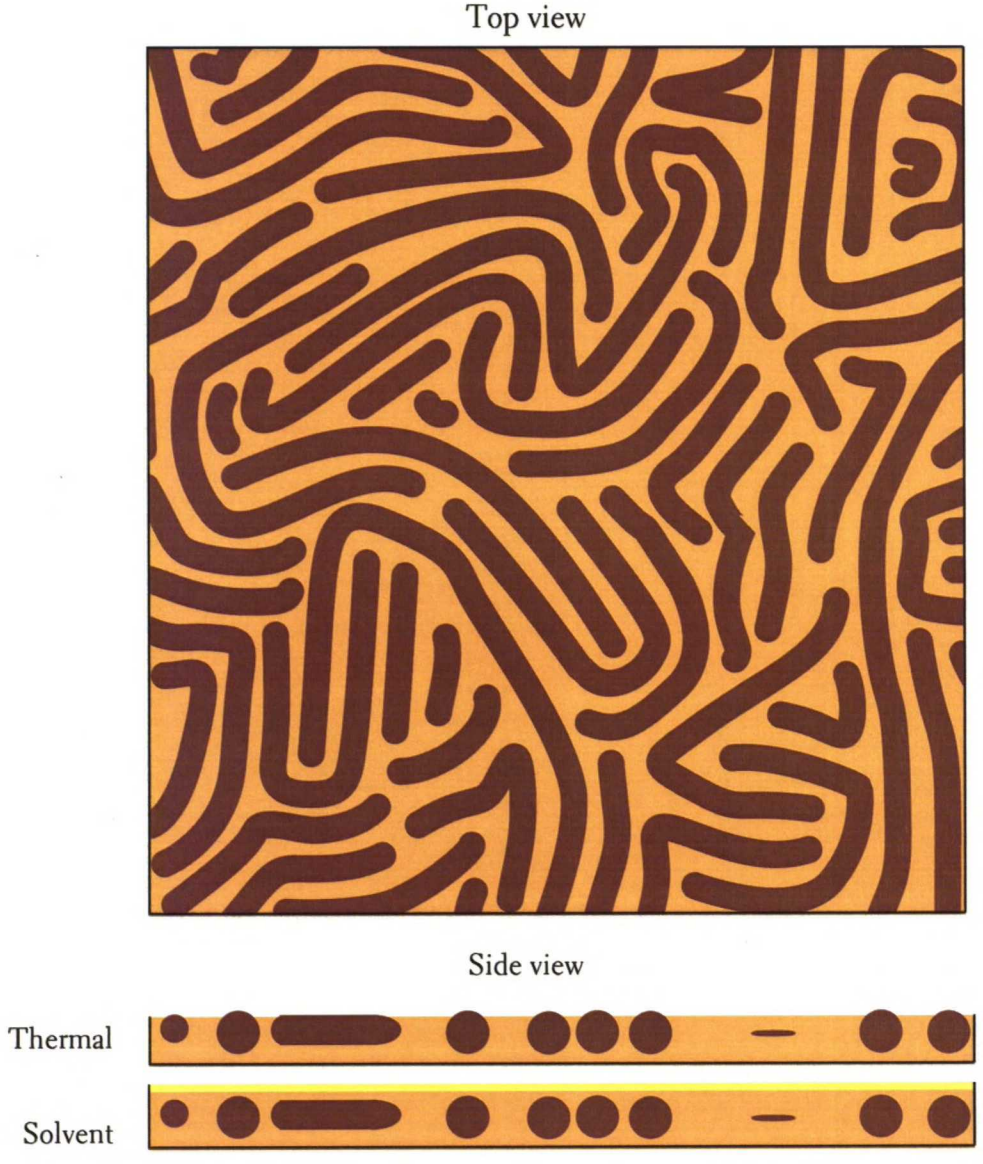

Figure 31. The proposed structure for annealed PS-*b*-PMMA thin films. The dark brown is the cylindrical component and the yellow matrix component. Top view and the separate side views show different results for different annealing methods. In ideal cases thermal annealing also produces cylindrical morphology parallel to the substrate but the difference to solvent annealing is the absence of the PS layer on top. The PS layer observed in solvent annealing is pictured bright yellow.

As observed earlier, changing the morphology from the PS cylinders in the PMMA matrix to the PMMA cylinders in the PS matrix does not change the morphology. Silicon and poly(imide) are both polar substrates and the more polar block likes to reside on the substrate and less polar on the air interface. Here PS is the less polar component and resides on the surface if only possible. In thermal annealing the films were too thin and the method inadequate to allow reasonable chain mobility to have PS layer on top. In SEM experiments a PS layer was observed to be the top layer. It appears that solvent annealing is superior over thermal annealing as a method. Equilibrium or near-equilibrium structures are obtained much quicker.

10.2 Poly(styrene)-*block*-poly(4-vinyl pyridine)

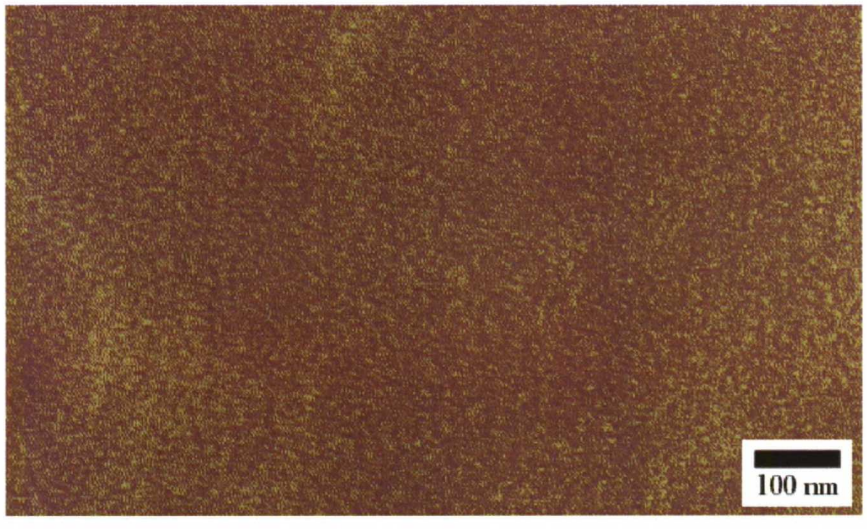

Figure 33. AFM phase image of PS-*b*-P4VP (#P112) on a silicon substrate. 1 w-% toluene solution was spun with 2000 rpm and the 40 nm thick film was annealed in 180 °C. The weight fraction of PS was 75 % and the expected morphology in bulk consists of P4VP cylinders in PS matrix. The AFM image was taken in Bayreuth with Multimode AFM. The phase image shows no contrast with only small interferences observable.

Both components in PS-*b*-P4VP block copolymers are in glassy state at the room temperature (glass transition temperatures of the blocks are 100 °C and 146 °C, respectively) and due to the similar hardness offer no phase contrast in AFM

measurements at ambient atmosphere. As is seen in Figure 33, the phase image shows no surface structure after thermal annealing. The exact reason why the phase images provide sufficient contrast with PS-*b*-PMMA and inadequate contrast with PS-*b*-P4VP remains yet unknown.

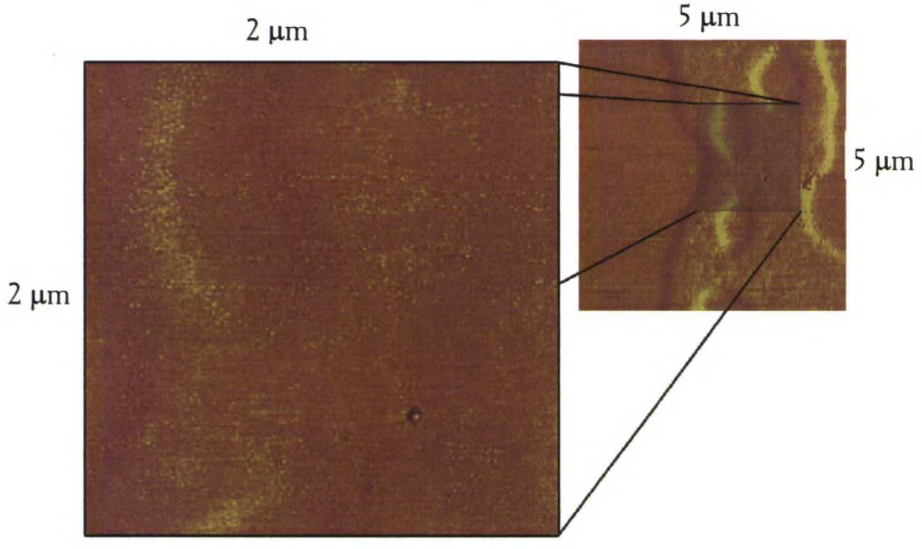

Figure 34. Example of a dewetting layer on top of the film, AFM phase image of PS-*b*-P4VP (#P99) on the silicon substrate. Polymer solution of 1 w-% in toluene was spun with 4000 rpm and annealed in chloroform for 13 h and $p_{chloroform}$= 0,8. The weight fraction of PS was 80 % with the expected morphology in bulk consists of P4VP cylinders in PS matrix. The AFM image was taken in Bayreuth with Dimension3000 and shows terracing due to a relatively high vapour pressure of the solvent. Note that the cylinder heads are seen mainly in the slope area between layers.

In solvent annealing experiments after annealing for more than 12 hours, the top-most layer of the film started to self-dewet and the formation of islands and holes started. Even though phase image shows no significant difference as seen in Figure 34, some cylinder heads are protruded on the film surface in despite of the layer of PS in the film-air interface.

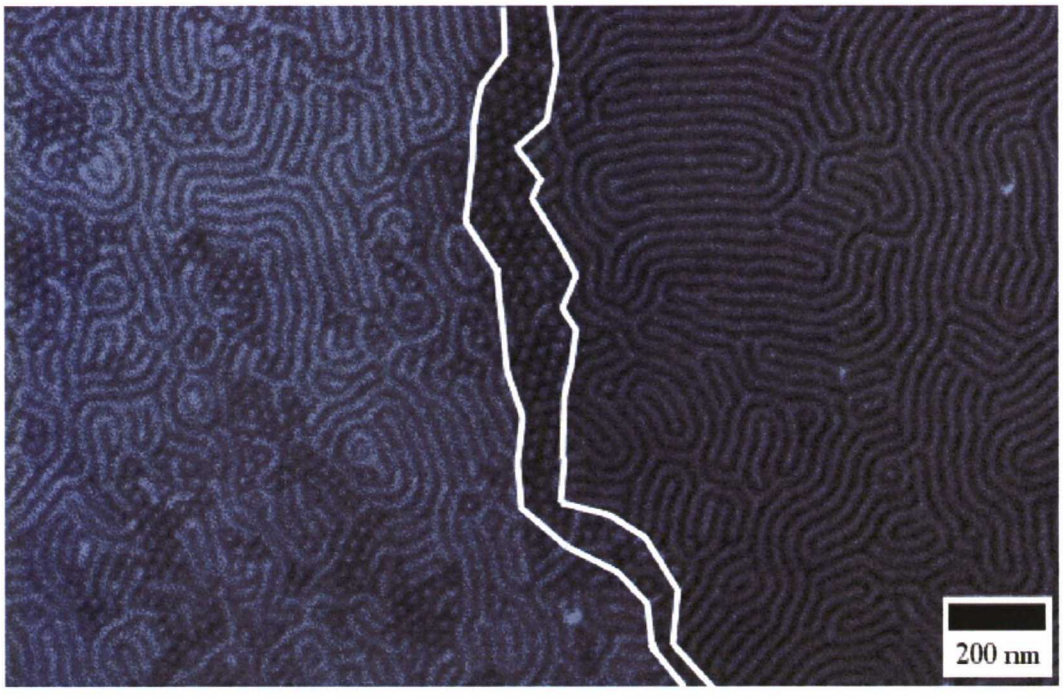

Figure 34. SEM image of annealed structure of PS-*b*-P4VP (#P99) thin film on silicon substrate. Specifications are the same as in Figure 33. Two terraces of film (difference of 25 nm) are seen and the slope between is marked with white lines. On the right side is observed whereas the topmost layer with P4VP cylinders parallel to the substrate, on the left the second layer with some cylinder heads perpendicular to the substrate are seen. The reason can be the poorer solvent contact or the surface effect of the polar substrate.

The film morphology was measured with SEM and observed to be parallel. The structure can be seen in Figure 34. On the right hand side is the top-most layer of the film and the second layer on the left. The top layer has completely parallel alignment due to the extensive contact with non-selective solvent, but in the second layer there are still cylinder heads visible. The slope between the layers is filled with cylinder heads. The morphology of the thin film is the same as in bulk and the level ordering depends on the contact time with the solvent.

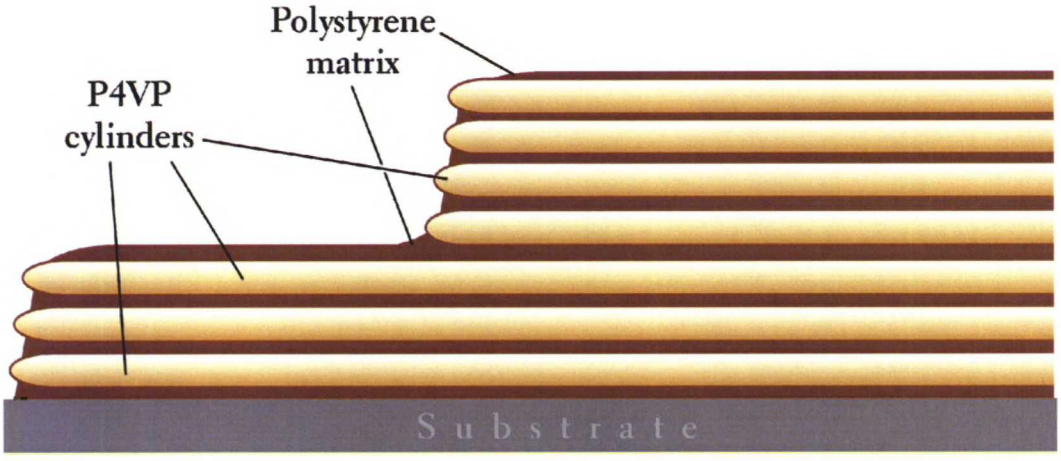

Figure 35. Proposed but yet unconfirmed structure for PS-*b*-P4VP thin films with expected morphology of the P4VP cylinders in the PS matrix on polar surfaces annealed with solvent for sufficiently long time. If pictured from below the film, picture would show the worm-like structure and the global alignment of these microdomains would require methods mentioned in Chapter 3.5.

In PS-*b*-PMMA system almost the same observations apply as in PS-*b*-P4VP system. With solvent annealing, the chloroform enhances the chain mobility greatly and the observed self-organised structure is parallel to the substrate. In solvent annealing experiments there is a set of parameters to vary: solution concentration, spinning speed, chloroform pressure, and the annealing time. A global parallel alignment might be achieved with a carefully chosen set of parameters. In Figure 35 is presented a schematic picture of a possible but yet unconfirmed structure. To achieve better structure and microdomain ordering, additional experiments are needed.

In literature Suh *et al.* [84] observed only parallel morphology in the system of deuterated PS and P2VP regardless of the film thickness on a silicon substrate. They indicated that P2VP has so strong an interaction with the silicon oxide substrate that the surface effects dominate the morphology making only the parallel morphology observable.

Solvent annealing is more efficient than thermal annealing due to the plasticising effect. If the perpendicular structure would be energetically more favourable than the parallel one, the final structure of solvent annealing would also be perpendicular. This

combined with the findings of Suh *et al.* indicate that the structures obtained with solvent annealing are near-to-equilibrium structures.

10.3 Poly(styrene)-*block*-poly(4-vinyl pyridine)·(pentadecylphenol)$_{1.0}$

Without PDP the both components of the polymer would be glassy, but PDP plasticises the P4VP phase. Only a small addition of PDP lowers the glass transition temperature significantly. After an addition of 0.15 PDP molecules per repeat unit of P4VP the glass transition temperature is 65 °C [85] In comparison, the glass transition temperature of the pure polymer is 146 °C. So the highest glass transition temperature of the blocks is with PS block. Unfortunately PDP becomes soluble in PS at about 130 °C. Solvent annealing was used instead.

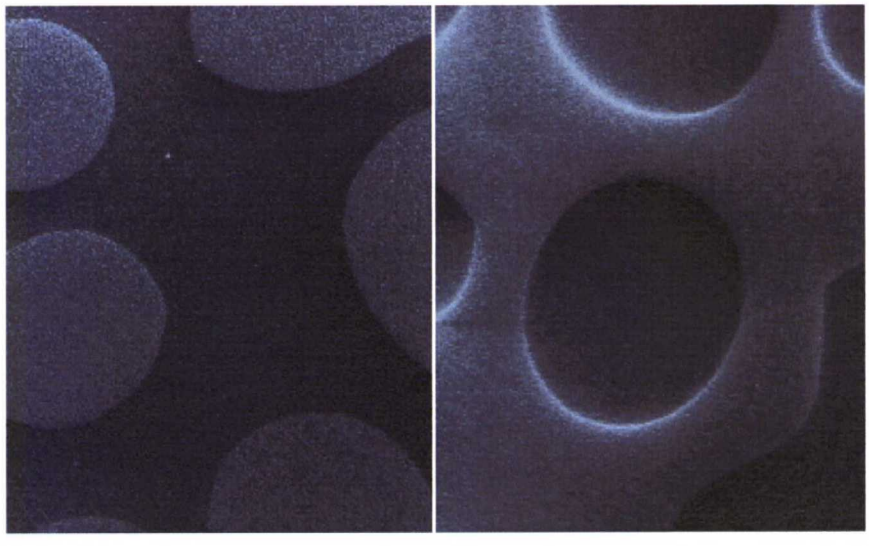

Figure 36. Island and hole formation on the surface of the PS-*b*-P4VP(PDP)$_{1.0}$ thin films observed with SEM. Films of 0.5 w-% of chloroform were spun with 4000-6000 rpm. Films were annealed for 12 h ($p_{chloroform}$= 0,7) in chloroform. On the left side, a layer of darker colour contains lighter islands and on the right a lighter blue layer has holes of darker blue in it. The step height was observed to be 16 nm high.

To a PS-*b*-P4VP polymer consisting of 8-9 w-% leading to P4VP spheres in PS matrix was added a nominal amount of one PDP molecule per P4VP repeat unit. In bulk PDP tunes the expected morphology from spherical to hierarchical lamellar-within-cylindrical

structure. By contrast the results in thin films showed, as seen in Figure 36, that the final morphology shows a distinctive island and hole formation. This behaviour usually alludes to a lamellar morphology. First assumption was as Suh et al. suggest that the vinyl pyridine block has so strong interaction with silicon and the structure is due to the strong polar substrate. Additional samples were prepared on a silicon substrate sputtered with 9 nm of carbon. But these carbon-coated substrates provided no change in surface structure and the assumption was rejected. The acceleration voltage of SEM was increased and this means that the electrons scattered deeper inside the film and the "inner" morphology was seen. The increase in acceleration voltage to almost tenfold provided nothing different compared to the surface findings. From this a conclusion was drawn that the observed surface structure is also the "inner" structure.

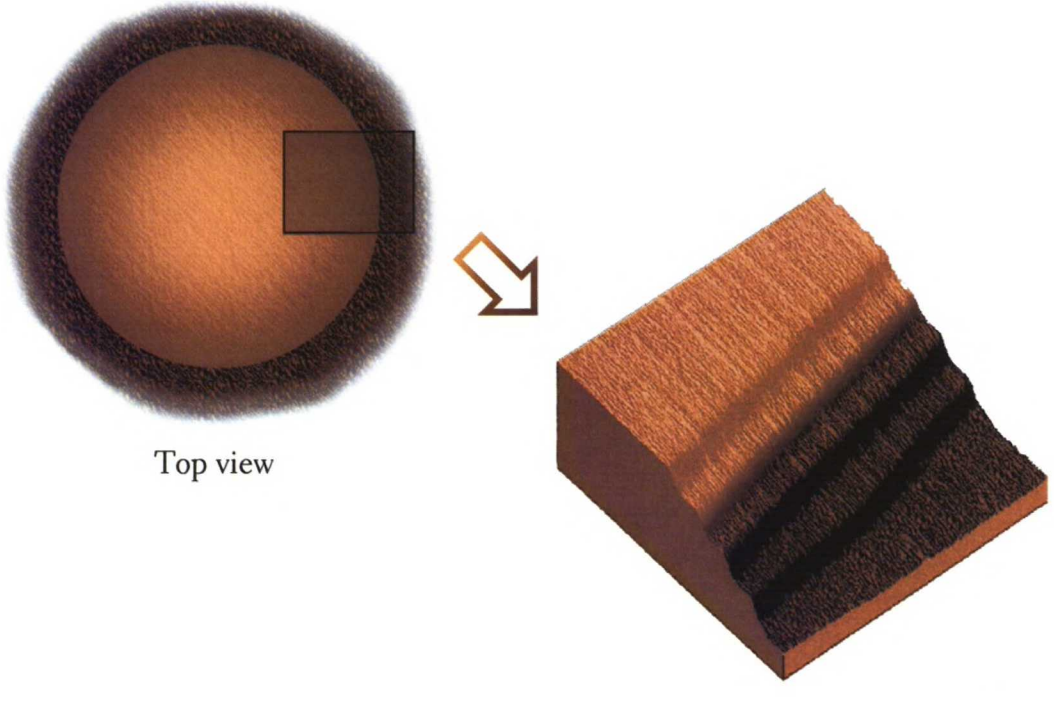

Figure 37. Scheme of the observed droplet formation on the top layer of PS-*b*-P4VP(PDP)$_{1.0}$ thin films spin coated with 6000 rpm from 0.5 w-% chloroform and annealed in for 18 h in $p_{chloroform}$=0,8. Droplets (light brown) were seen on surface (dark brown). The excerpt from the droplet shows the step-like formation of layers. Layer thickness was observed to be the same as in SEM measurements in Figure 36.

In further tests with solvent annealing a higher partial pressure of chloroform was applied to maximise the chain mobility. Significant self-dewetting and droplet formation was observed on the top layer of the film. After quenching the structure, droplets were seen to be round stepwise structures as seen in Figure 37.

There are three possible explanations for the observation of lamellar structure. One of the explanations is that the PDP phase is not microphase-separated and the structure is as seen in Figure 38. This purely lamellar structure would be possible due to that the side-chain crystallisation in thin films has not been examined thoroughly.

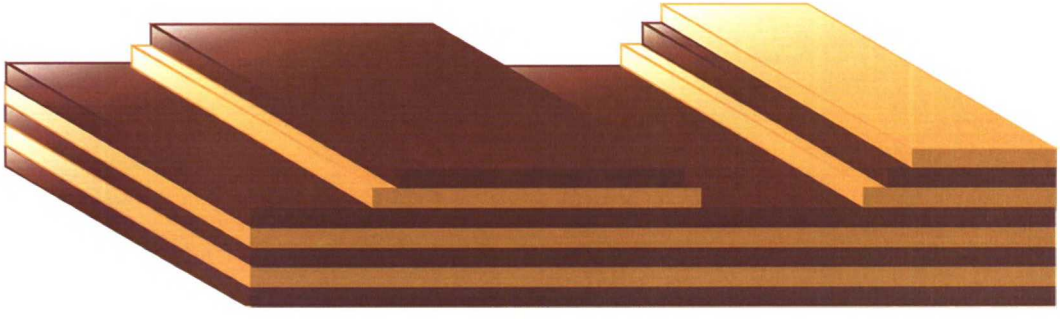

Figure 38. The schematised proposed structure of PS-*b*-P4VP(PDP)$_{1.0}$ thin films. The top layers self-dewet to form droplets and the step-like is seen on the surface of the structure.

Another explanation for the structure would be the PDP leaving the structure. Reason could be the mixed solvent effect of PDP and chloroform or the combination of phase separation and a non-selective solvent. This would leave the thin films with the expected structure of P4VP spheres in PS matrix. However, the surface effects demand a layer of PS in both interfaces. These restrictions reduce the amount of PS and might enable the formation of the lamellar structure in thin film. These two explanations are highly speculative and do not seem very probable.

The most probable explanation is that the lamellar structure is a hierarchical structure of lamellar-within-lamellar. The effect that forces the lamellar-within-cylindrical structure to lamellar-within-lamellar is so-called side-chain crystallisation. Lyuten *et al.* observed

that the crystallisation temperature of P4VP(PDP)$_{1.0}$ block is 28 °C and according to Ruokolainen *et al.* the order-disorder transition is 60 °C. [85, 86] The crystallisation temperature is lower than would be the T_G of the material. Diblock copolymer's crystallising component alters the morphology of the film, because crystallisation destroys the ordered melt morphology. The smaller structure cannot be observed at the moment and requires further studies. [17] In Figure 39 is a proposed but yet unconfirmed structure. If this conclusion is true, the hydrogen bonding is a route to supramolecular structures that has not been published so far. In order to address this problem, further studies are required with AFM equipped with a thermal controller in the sample holder.

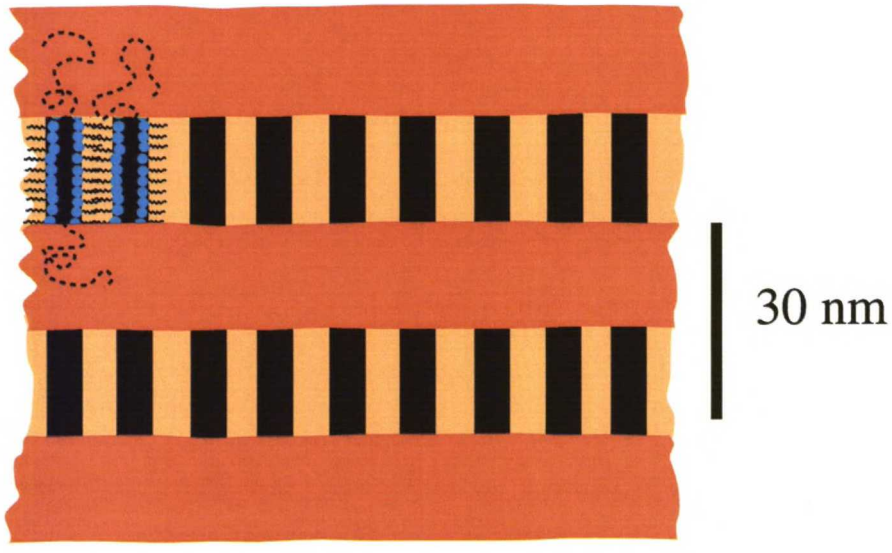

Figure 39. The schematic structure of lamellar-within-lamellar hierarchical morphology: the orange colour represents the PS lamellar layer, the light brown colour represents the PDP phase and the black colour the P4VP phase. Blue circles represent the phenol group of PDP.

11 CONCLUSIONS

In the scope of this work, three different block copolymer polymer thin film systems were studied on two different substrate materials with two different annealing methods.

Several factors and their influence in thin film structure alignment were identified. First the AFM was established as a method with a PS-b-PMMA. It was found that changing the substrate material showed no significant change in the morphology. Film thickness and the annealing method were observed to play a key role in the alignment of the structures. In ultrathin films with thickness of less than a complete repeat thickness the thermal annealing is not adequate method to align structures in comparison with the solvent annealing. Elevated temperature seems to produce kinetically trapped structures with a local energy minimum but with the solvent annealing method the chain mobility was found to be sufficient to produce equilibrium or near-equilibrium structures.

Secondly thin films were manufactured with material, which allows structural hierarchy upon introducing. PS-*b*-P4VP was introduced with PDP to form hierarchical structures. Three possible explanations to the observed lamellar structure were defined. The expected bulk structure of lamellar-within-cylindrical was not observed, instead a hierarchical structure of lamellar-within-lamellar was observed due to the side-chain crystallisation. The more unlikely explanations for the structure are that PDP has left the structure or the combination of surface effects induces lamellar morphology. This is yet highly speculative and further studies are needed.

AFM was introduced as a worthwhile method to study thin films with sufficient phase contrast or surface structures. PS-*b*-P4VP and PS-*b*-P4VP(PDP)$_{1.0}$ materials provide no phase contrast in AFM and PS-*b*-PMMA does. This matter is not trivial and the reason remains unknown. For materials with insufficient phase contrast in AFM, SEM was found to be an extremely useful tool.

In conclusion, AFM was found to be a very useful tool in investigating block copolymer structures and the first evidence of hierarchical structures in thin films were identified.

12 SUBJECTS FOR FURTHER INVESTIGATION

Several areas of this thesis require further investigation. Introduction of AFM was successful and the next logical task is to construct similar experiment set-up of solvent annealing to the laboratory of Optics and Molecular Materials as the one used in The Bayreuth University.

For PS-*b*-PMMA system a complete dependency of the spinning speed versus film thickness would be useful. In order to fully utilise the potential of block copolymer thin films, orientation methods would have to be used. For example orientation with electric fields might produce upright cylinders. With these films the application possibilities of upright cylinder morphology are endless. With the degradation of PMMA, a surface with nanopores could be introduced. The pores could be filled with conducting metals like gold and obtain anisotropic conducting properties. Changing the material could lead to the controlled release of drugs through the pores or even artificial dialysis.

With ultrathin films and reverting the matrix one could obtain nano-sized upright cylinders with possible applications such as the lotus effect.

With PS-*b*-P4VP one could try the orientation with electric fields or shear orientation. Further subject could be to attach a chelate to the nitrogen of the pyridine ring and obtain a catcher for heavy metals. These materials would have large functionality per specific weight. Although with zeolites this area is under heavy research, some applications might be handy with block copolymer thin films also.

With hierarchical structures one could obtain the expected bulk morphologies instead of lamellar structures by studying the materials on elevated temperatures and quenching the structure quickly so that the amorphous component would not have the time to crystallise. This would require additional equipment to the existing AFM equipment.

13 REFERENCES

1. Whitesides, G.M., Self-Assembling Materials, *Sci. Am.* **273** (1995) 114-127.
2. Whitesides, G.M., and Love, J.C., The Art of Building Small, *Sci. Am.* **285** (2001) 39-47.
3. Muthukumar, M., Ober, C.K., and Thomas, E.L., Competing Interactions and Levels of Ordering in Self-Organizing Polymeric Materials, *Science* **277** (1997) 1225-1232.
4. Stupp, S., and Braun, P.V., Molecular Manipulation of Microstructures: Biomaterials, Ceramics and Semiconductors, *Science* **277** (1997) 1242-1247.
5. Whitesides, G.M., Mathias, J.P., and Seto, C.T., Molecular Self-Assembly and Nanochemistry: A Chemical Strategy for the Synthesis of Nanostructures, *Science* **254** (1991) 1312-1319.
6. Whitesides, G.M., and Grzybowski, B., Self-Assembly at All Scales, *Science* **295** (2002) 2418-2421.
7. Bates, F.S., and Fredrickson, G.H., Block Copolymer Thermodynamics: Theory and Experiment, *Annu. Rev. Phys. Chem.* **41** (1990) 525-549.
8. Bates, F.S., and Fredrickson, G.H., Block Copolymer - Designer Soft Materials, *Physics Today* **52** (1999) 32-38.
9. Fredrickson, G.H., and Bates, F.S., Dynamics of Block Copolymers: Theory and Experiment, *Annu. Rev. Mater. Sci.* **26** (1996) 501-550.
10. Chen, Z., and Kornfield, J.A., Flow-induced alignment of lamellar block copolymer melts, *Polymer* **39** (1998) 4679-4699.
11. Rehahn, M., Organic/inorganic hybrid polymers, *Acta Pol.* **49** (1998) 201-224.
12. Sijbesma, R.P., Beijer, F.H., Brunsveld, L., Folmer, B.J.B., Hirschberg, J.H.K.K., Lange, R.F.M., Lowe, J.K.L., and Meijer, E.W., Reversible Polymers Formed from Self-Complementary Monomers Using Quadruple Hydrogen Bonding, *Science* **278** (1997) 1601-1604.
13. Yu, S.M., Conticello, V.P., Zhang, G., Kayser, C., Fournier, M.J., Mason, T.L., and Tirrell, D.A., Smectic ordering in solutions and films of a rod-like polymer owing to monodispersity of chain length, *Nature* **389** (1997) 167-170.
14. Gedde, U.W., *Polymer Physics*, 1st ed., Chapman & Hall, London 1995, 298 p.

15. Seppälä, J., *Polymeeriteknologian Perusteet*, 3rd ed., Otatieto, Espoo 1999, 267 p.

16. Birley, A.W., Haworth, B., and Batchelor, J., *Physics of Plastics*, Carl Hanser Verlag, Königsfeld 1992, 571 p.

17. Hamley, I.W., *The Physics of Block Copolymers*, 1st ed., Oxford University Press, Oxford 1998, 422 p.

18. Ruokolainen, J., ten Brinke, G., and Ikkala, O., Supramolecular Polymeric Materials with Hierarchical Structure-Within-Structure, *Adv. Mat.* **11** (1999) 777-780.

19. Laurer, J.H., Hajduk, D.A., Dreckoetter, S., Smith, S.D., and Spontak, R.J., Bicontinuous Morphologies in Homologous Multiblock Copolymers and Their Homopolymer Blends, *Macromolecules* **31** (1998) 7546-7549.

20. Zheng, W., and Wang, Z., Morphology of ABC Triblock Copolymers, *Macromolecules* **28** (1995) 7215-7223.

21. Krappe, U., Stadler, R., and Voigt-Martin, I., Chiral Assembly in Amorphous ABC Triblock Copolymers. Formation of a Helical Morphology in Polystyrene-block-polybutadiene-poly(methyl methacrylate) Block Copolymers, *Macromolecules* **28** (1995) 4558-4561.

22. Ringsdorf, H., Voigt-Martin, I., Wendorff, J., Wüstefeld, R., and Zentel, R., Molecular Engineering of Liquid Crystalline Polymers. In *Chemistry and Physics of Macromolecules*, E.W. Fischer, R.C. Schulz, and H. Silescu, Eds., VCH Verlagsgesellschaft mbH, Weinheim 1991, pp. 213.

23. Stryer, L., *Biochemistry*, 4th ed., W.H. Freeman & Co., New York 1995, 1224 p.

24. Zubay, G., *Biochemistry*, 3rd ed., Wm. C. Brown Publishers, Dubuque 1993, 1024 p.

25. Hamley, I.W., *Introduction to Soft Matter*, 1st ed., John Wiley & Sons, New York 2000, 342 p.

26. Keller, A., Warner, M., and Windle, A.H., Self-Order and Form in Polymeric Materials. In *Phase Morphology in Block Copolymer Systems*, E.L. Thomas, and R.L. Lescanec, Eds., Chapman & Hall, London 1995, pp. 147-164.

27. ten Brinke, G., From Homopolymers to Random Multiblock Copolymers: An Introduction to the Theory of Microphase Separation, Helsinki University of Technology, Department of Technical Physics and Mathematics, Espoo 2002, 65 p.

28. Seul, M., and Andelman, D., Domain Shapes and Patterns: The Phenomenology of Modulated Phases, *Science* **267** (1995) 476-482.

29. Anastasiadis, S.H., and Russell, T.P., Neutron Reflectivity Studies of the Surface-Induced Ordering of Diblock Copolymer Films, *Phys. Rev. Lett.* **62** (1989) 1852-1855.

30. Matsen, M.W., and Bates, F.S., Unifying Weak- and Strong-Segregation Block Copolymer Theories, *Macromolecules* **29** (1996) 1091-1098.

31. Ruotsalainen, T., Nanohuokoisten materiaalien valmistaminen hierarkisten polymeeristen supramolekyylien avulla, Master's Thesis, Helsinki University of Technology, Department of Chemical Technology, Espoo 2002, 91 p.

32. Elbs, H., Abetz, V., Hadziioannou, G., Drummer, C., and Krausch, G., Antiferromagnetic Ordering in a Helical Triblock Copolymer Mesostructure, *Macromolecules* **34** (2001) 7917-7919.

33. Chen, Z., Issalan, A., M., Kornfield, J., Smith, S.D., Grothaus, J.T., and Satkowski, M.M., Dynamics of Shear-Induced Alignment of a Lamellar Diblock: A Rheo-optical, Electron Microscopy, and X-Ray Scattering Study, *Macromolecules* **30** (1997) 7096-7114.

34. Mäki-Ontto, R., Flow and Conductivity Properties of Comb-Shaped Self-Organised Supramolecules, Doctoral Thesis, Helsinki University of Technology, Department of Engineering Physics and Mathematics, Espoo 2001.

35. Thurn-Albrecht, T., DeRouchey, J., and Russell, T.P., Overcoming Interfacial Tensions with Electric Fields, *Macromolecules* **33** (2000) 3250-3253.

36. Morkved, T.L., Lu, M., Urbas, A.M., Ehrichs, E.E., Jaeger, H.M., Mansky, P., and Russell, T.P., Local Control of Microdomain Orientation in Diblock Copolymer Thin Films with Electric Fields, *Science* **273** (1996) 931-933.

37. Mansky, P., DeRouchey, J., Russell, T.P., Mays, J., Pitsikalis, M., Morkved, T., and Jaeger, H., Large-Area Domain Alignment in Block Copolymer Thin Films Using Electric Fields, *Macromolecules* **31** (1998) 4399-4401.

38. Gurovich, E., Why does an Electric Field Align Structures in Copolymers?, *Phys. Rev. Lett.* **74** (1995) 482-485.

39. Böker, A., Elbs, H., Hänsel, H., Knoll, A., Ludwigs, S., Zettl, H., Krausch, G., Urban, V., Abetz, V., and Müller, A.H.E., Macroscopic Alignment of Concentrated Block Copolymer Solutions in Electric Fields., *Polymer Preprints* **43** (2002) 377-378.

40. Fujiwara, M., Fukui, M., and Tanimoto, Y., Magnetic Orientation of Benzophenone Crystals in Fields up to 80.0 KOe, *J. Phys. Chem. B* **103** (1999) 2627-2630.

41. Sata, H., Kimura, T., Ogawa, S., Yamato, M., and Ito, E., Magnetic orientation of poly(ethylene-2,6-naphthlate), *Polymer* **37** (1996) 1879-1882.

42. Sata, H., Kimura, T., Ogawa, S., and Ito, E., Magnetic orientation of poly(ethylene-2,6-naphthlate) during crystallization from melt, *Polymer* **39** (1998) 6325-6330.

43. Kawaii, T., and Kimura, T., Magnetic orientation of isotactic polypropylene, *Polymer* **41** (2000) 155-159.

44. Gupta, V.K., Krishnamoorti, R., Kornfield, J.A., and Smith, S.D., Evolution of microstructure during shear alignment in a polystyrene-isoprene lamellar diblock copolymer, *Macromolecules* **28** (1995) 4464-4474.

45. Assender, H.E., and Windle, A.H., The relaxation of a magnetically orientated liquid crystalline polymer, *Polymer* **37** (1996) 371-375.

46. Kim, G., and Libera, M., Morphological Development in Solvent-Cast Polystyrene-Polybutadiene-Polystyrene (SBS) Triblock Copolymer Thin Films, *Macromolecules* **31** (1998) 2569-2577.

47. Knoll, A., Horvat, A., Lyakhova, K.S., Krausch, G., Sevink, G.J.A., Zvelindovsky, A.V., and Magerle, R., Phase Behavior in Thin Films of Cylinder Forming Block Copolymers, *Phys. Rev. Lett.* **89** (2001) 035501- 1 - 035501-4.

48. Fasolka, M.J., Harris, D.J., Mayes, A.M., Yoon, M., and Mochrie, S.G.J., Observed Substrate Topography-Mediated Lateral Patterning of Diblock Copolymer Films, *Phys. Rev. Lett.* **79** (1997) 3018-3021.

49. Huang, E., Russel, T.P., Harrison, C., Chaikin, P.M., Register, R.A., Hawker, C.J., and Mays, J., Using Surface Active Random Copolymers to Control the Domain Orientation in Diblock Copolymer Thin Films, *Macromolecules* **31** (1998) 7641-7650.

50. Konrad, M., Knoll, A., Krausch, G., and Magerle, R., Volume Imaging of an Ultrathin SBS Triblock Copolymer Film, *Macromolecules* **33** (2000) 5518-5523.

51. Huang, E., Pruzinsky, S., Russell, T.P., Mays, J., and Hawker, C.J., Neutrality Conditions for Block Copolymer Systems on Random Copolymer Brush Surfaces, *Macromolecules* **32** (1999) 5299-5303.

52. Morkved, T.L., and Jaeger, H.M., Thickness-induced morphology changes in lamellar diblock ultrathin films, *Europhys. Lett.* **40** (1997) 643-648.

53. Fasolka, M.J., and Mayes, A.M., Block Copolymer Thin Films: Physics and Applications, *Annu. Rev. Mater. Res.* **31** (2001) 323-55.

54. Mansky, P., Russell, T.P., Hawker, C.J., Pitsikalis, M., and Mays, J., Ordered Diblock Copolymer Films on Random Copolymer Brushes, *Macromolecules* **30** (1997) 6810-6813.

55. Lammertink, R.G.H., Hempenius, M.A., Vancso, G.J., Shin, K., Rafailovich, M.H., and Sokolov, J., Morphology and Surface Relief Structures of Asymmetric Poly(styrene-block-ferrocenylsilane) Thin Films, *Macromolecules* **34** (2001) 942-950.

56. Heier, J., Kramer, E.J., Walheim, S., and Krausch, G., Thin Diblock Copolymer Films on Chemically Heterogeneous Surfaces, *Macromolecules* **30** (1997) 6610-6614.

57. Green, P.F., and Limary, R., Block copolymer thin films: pattern formation and phase behavior, *Adv. Coll.* **94** (2001) 53-81.

58. Singh, N., Kudrle, A., Sikka, M., and Bates, F.S., Surface Topography of Symmetric and Asymmetric Polyolefin Block Copolymer Thin Films, *J. Phys. II France* **5** (1995) 377-96.

59. Maaloum, M., Ausserre, D., Chatenay, D., Coulon, G., and Gallot, Y., Edge Profile of Relief 2D Domains at the Free Surface of Smectic Copolymer Thin Films, *Phys. Rev. Lett.* **68** (1992) 1575-1578.

60. Coulon, G., Collin, B., Ausserre, D., Chatenay, D., and Russell, T.P., Islands and holes on the free surface of thin diblock copolymer films. I. Characteristics of formation growth, *J. Phys. France* **51** (1990) 2801-2811.

61. Anon., *A Practical Guide to Scanning Probe Microscope*, 2000, ThermoMicroscopes.

62. Anon., *Scanning Probe Microscopy Training Notebook*, 2002, Digital Instruments, Santa Barbara.

63. Heaton, M.G., and Serry, F.M., *Scanning Probe/Atomic Force Microscopy: Technology Overview and Update*, 2002, Digital Instruments.

64. Babcock, K.L., and Prater, C.B., *Phase Imaging: Beyond Topography*, 2002, Digital Instruments.

65. Anon., *All you wanted to know about Electron Microscopy, but didn't know what to ask*, 1995, Philips.

66. Crewe, A.V., Electron Microscopy. In *Encyclopedia of Physics*, R.G. Lerner, and G.L. Trigg, Eds., Addison-Wesley Publishing Company, Inc., Reading 1981, pp. 256-257.

67. Callister Jr., W.D., *Materials Science and Engineering: An Introduction*, John Wiley Sons, Inc., New York 1999, 85 p.

68. Ezer, Y., *Introduction to Scanning Electron Microscopy (SEM)*, 1997, Postgraduate Seminar Lecture: Otaniemi. p. 36.

69. Goldstein, J.I., Newbury, D.E., Echlin, P., Joy, D.C., Fiori, C., and Lifshin, E., *Scanning Electron Microscopy and X-Ray Microanalysis*, Plenum Press, New York 1984, 650 p.

70. Sperling, L.H., *Introduction to Physical Polymer Science*, John Wiley & Sons, Inc., New York 2001, 671 p.

71. Cosandey, F., High resolution/low voltage SEM, *Advanced Materials & Processes* (1999) 37-39.

72. Vezie, D.L., Thomas, E.L., and Adams, W.W., Low-voltage, high-resolution scanning electron microscopy: a new characterization technique for polymer morphology, *Polymer* **36** (1995) 1761-1779.

73. Keränen, *Nykyaikainen mikroskopia ja sen tarjoamat mahdollisuudet*, 1997, TTKK: Tampere.

74. Harrison, C., Park, M., Chaikin, P., Register, R.A., Adamson, D.H., and Yao, N., Depth Profiling Block Copolymer Microdomains, *Macromolecules* **31** (1998) 2185-2189.

75. Ruokolainen, J., Saariaho, M., Ikkala, O., ten Brinke, G., Thomas, E.L., Torkkeli, M., and Serimaa, R., Supramolecular Routes to Hierarchical Structures: Comb-Coil Diblock Copolymers Organized with Two Length Scales, *Macromolecules* **32** (1999) 1152-1158.

76. Russell, T.P., Coulon, G., Deline, V.R., and Miller, D.C., Characteristics of the surface-induced orientation for symmetric diblock PS/PMMA copolymers, *Macromolecules* **22** (1989) 4600-4606.

77. Smith, A.P., Douglas, J.F., Meredith, J.C., Amis, E.J., and Karim, A., Combinatorial Study of Surface Pattern Formation in Thin Block Copolymer Films, *Phys. Rev. Lett.* **87** (2001) 015503/1-015503/4.

78. Stocker, W., Beckmann, J., Stadler, R., and Rabe, J.P., Surface Reconstruction of the Lamellar Morphology in a Symmetric Poly(styrene-block-butadiene-block-methyl methacrylate) Triblock Copolymer: A Tapping Mode Scanning Force Microscope Study, *Macromolecules* **29** (1996) 7502-7507.

79. Rharbi, Y., and Winnik, M.A., Interface Thickness of a Styrene-Methyl Methacrylate Block Copolymer in the Lamella Phase by Direct Nonradiative Energy Transfer, *Macromolecules* **34** (2001) 5238-5248.

80. Sohn, B.H., and Yun, S.H., Perpendicular lamellae induced at the interface of neutral self-assembled monolayers in thin diblock copolymer films, *Polymer* **43** (2002) 2507-2512.

81. Leibler, L., Theory of Microphase Separation in Block Copolymers, *Macromolecules* **13** (1980) 1602-1617.

82. Jones, D.J., Smith, J.R., Huck, W.T.S., and Alexander, C., Variable Adhesion of Micropatterned Thermoresponsive Polymer Brushes: AFM Investigations of Poly(N-isopropylamide) Brushes Prepared by Surface-Initiated Polymerizations, *Adv. Mat.* **14** (2002) 1130-1134.

83. Ruokolainen, J., Mäkinen, R., Torkkeli, M., Mäkelä, T., Serimaa, R., ten Brinke, G., and Ikkala, O., Switching Supramolecular Polymeric Materials with Multiple Length Scales, *Science* **280** (1998) 557-560.

84. Suh, K.Y., Kim, Y.S., and Lee, H.H., Parallel and Vertical Morphologies in Block Copolymers of Cylindrical Domain, *J. Chem. Phys.* **108** (1998) 1253-1256.

85. Luyten, M.C., Alberda, G.O.R., van Ekenstein, A., Wildeman, J., ten Brinke, G., Ruokolainen, J., Ikkala, O., Torkkeli, M., and Serimaa, R., Crystallization and Co-crystallization in Supramolecular Comb Copolymer-like Systems: Blends of Poly(4- vinylpyridine) and Pentadecylphenol, *Macromolecules* **32** (1999) 4404-4410.

86. Ruokolainen, J., Torkkeli, M., Serimaa, R., Komanschek, E., Ikkala, O., and ten Brinke, G., Order-Disorder Transition in Polymer-Surfactant Systems, *Phys. Rev. E* **54** (1996) 6646-6649.


TEKNILLINEN KORKEAKOULU
KEMIAN TEKNIIKAN OSASTO